

Spectrum Occupancy Measurements of the 3550–3650 Megahertz Maritime Radar Band near San Diego, California

**Michael Cotton
Roger Dalke**



report series

Spectrum Occupancy Measurements of the 3550–3650 Megahertz Maritime Radar Band near San Diego, California

**Michael Cotton
Roger Dalke**



U.S. DEPARTMENT OF COMMERCE

January 2014

DISCLAIMER

Certain commercial equipment, instruments, or materials are identified in this report to adequately describe the experimental procedure. In no case does such identification imply recommendation or endorsement by the National Telecommunications and Information Administration, nor does it imply that the material or equipment identified is necessarily the best available for the purpose.

ACKNOWLEDGEMENTS

This investigation required the services of a number of ITS engineers, some of whom are not included in the list of authors. The authors recognize Frank Sanders for his overall expertise in radar systems and his complete understanding of spectrum analyzer functionality especially for the purpose of radar detection. The authors also acknowledge Geoff Sanders for the development of software for instrument control, Jeffery Wepman for his expertise in test and measurement equipment, and Paul McKenna for his knowledge of radiowave propagation.

CONTENTS

List of Figures	vii
List of Tables	ix
Variables and Acronyms.....	x
1 Introduction.....	1
1.1 Background.....	2
1.2 Organization of this Report.....	2
2 SPN-43 System Description	4
3 Measurement Strategy	5
3.1 System Description	5
3.2 Measurement Procedure	6
3.2.1 System Calibration	6
3.2.2 Frequency-Swept Occupancy Measurements	8
3.2.3 Time-Domain Signal Characterization Measurements	9
3.3 Range of Detection	11
4 Observed Signal Patterns	13
4.1 Calibration Data.....	13
4.2 Measurement Time Resolution.....	14
4.3 Spectrogram of Full Frequency-Swept Data Set	14
5 Statistical Considerations for Spectrum Occupancy Measurements	17
5.1 Renewal Theory and the Definition of Channel Occupancy	17
5.2 Estimation of Channel Occupancy	18
5.3 Estimation of Band Occupancy	19
6 Measurement Results.....	21
6.1 Band Occupancy.....	21
6.1.1 Daily Means	21
6.1.2 Two-Week Statistics.....	22
6.2 Channel Occupancy	24
6.2.1 Example Calculations.....	24
6.2.2 Channel Occupancy Statistics versus Frequency	25
6.3 Time Intervals	27
7 Summary	31
8 References.....	32
APPENDIX A: Channel Occupancy in the Context of Renewal Theory.....	33
A.1 Setup	33
A.2 Satisfying the Renewal Equation.....	34

A.3 Asymptotic Behavior of the Renewal Process	36
APPENDIX B: Confidence Intervals for Channel Occupancy Estimates	37
B.1 Assuming Independent Sampling in Time	38
B.2 Assuming Dependent Sampling in Time	39
APPENDIX C: Daily Signal-Level and Band Occupancy Plots	42

LIST OF FIGURES

Figure 1. S-Band radar spectrum.	4
Figure 2. Block diagram of radar occupancy measurement system.	5
Figure 3. Peak-to-average ratio of complex Gaussian noise versus dwell time and bandwidth.....	7
Figure 4. Example frequency-swept occupancy measurement.....	8
Figure 5. Example rotation period measurement.....	10
Figure 6. Example pulse-interval measurement.....	10
Figure 7. Example pulse-width measurement.....	11
Figure 8. Irregular Terrain Model predictions of basic transmission loss versus range and distance to line-of-sight edge for different terminal heights.....	12
Figure 9. (Top) Calibration data acquired during San Diego measurement and (Bottom) maximum measured power levels compared to system dynamic range.....	13
Figure 10. Probability distribution of time between measurements.	14
Figure 11. Measured signals in the 3.6 MHz band on June 8–21, 2012, near San Diego.	16
Figure 12. Channel transmissions and related time intervals.	17
Figure 13. Probability distributions of band occupancy measured during weekdays on June 8–21, 2012, near San Diego.....	23
Figure 14. Probability distributions of band occupancy measured during weekends on June 8–21, 2012, near San Diego.....	23
Figure 15. Transition probability ($L = -83$ dBm) versus frequency on June 8–21, 2012, near San Diego.....	26
Figure 16. Channel occupancy estimates ($L = -83$ dBm) with 90% confidence intervals versus frequency on June 8–21, 2012, near San Diego.	26
Figure 17. Channel occupancy estimates versus frequency at various threshold levels on June 8–21, 2012, near San Diego.....	27
Figure 18. Measured mean transmission intervals ($L = -83$ dBm) versus frequency on June 8–21, 2012, near San Diego.....	28
Figure 19. Probability distributions of transmission intervals ($f = 3.59$ GHz, $L = -83$ dBm) measured during weekdays on June 8–21, 2012, near San Diego. Dashed lines are corresponding exponential distributions.	29
Figure 20. Probability distributions of transmission intervals ($f = 3.57$ GHz, $L =$ -83 dBm) measured during weekdays on June 8–21, 2012, near San Diego. Dashed lines are corresponding exponential distributions.....	30
Figure A-1. Renewal process $X(t)$ and associated transmission interval random variables.	33
Figure A-2. Sample function of a renewal process.....	34
Figure B-1. Illustration of confidence interval (c_1, c_2) for parameter p	38
Figure B-2. $D(\varepsilon)$ for $N = 738$ and $\varepsilon = 0.1$ demonstrating the difference between independent and dependent sampling.	41
Figure C-1. M4 statistics of 3550–3650 MHz spectrum measured near San Diego on June 8, 2012.....	43
Figure C-2. Spectrogram and band occupancy for 3550–3650 MHz spectrum measured near San Diego on June 8, 2012.....	43
Figure C-3. M4 statistics of 3550–3650 MHz spectrum measured near San Diego on June 9, 2012.....	44

Figure C-4. Spectrogram and band occupancy for 3550–3650 MHz spectrum measured near San Diego on June 9, 2012.....	44
Figure C-5. M4 statistics of 3550–3650 MHz spectrum measured near San Diego on June 10, 2012.....	45
Figure C-6. Spectrogram and band occupancy for 3550–3650 MHz spectrum measured near San Diego on June 10, 2012.....	45
Figure C-7. M4 statistics of 3550–3650 MHz spectrum measured near San Diego on June 11, 2012.....	46
Figure C-8. Spectrogram and band occupancy for 3550–3650 MHz spectrum measured near San Diego on June 11, 2012.....	46
Figure C-9. M4 statistics of 3550–3650 MHz spectrum measured near San Diego on June 12, 2012.....	47
Figure C-10. Spectrogram and band occupancy for 3550–3650 MHz spectrum measured near San Diego on June 12, 2012.....	47
Figure C-11. M4 statistics of 3550–3650 MHz spectrum measured near San Diego on June 13, 2012.	48
Figure C-12. Spectrogram and band occupancy for 3550–3650 MHz spectrum measured near San Diego on June 13, 2012.....	48
Figure C-13. M4 statistics of 3550–3650 MHz spectrum measured near San Diego on June 14, 2012.	49
Figure C-14. Spectrogram and band occupancy for 3550–3650 MHz spectrum measured near San Diego on June 14, 2012.....	49
Figure C-15. M4 statistics of 3550–3650 MHz spectrum measured near San Diego on June 15, 2012.	50
Figure C-16. Spectrogram and band occupancy for 3550–3650 MHz spectrum measured near San Diego on June 15, 2012.....	50
Figure C-17. M4 statistics of 3550–3650 MHz spectrum measured near San Diego on June 16, 2012.	51
Figure C-18. Spectrogram and band occupancy for 3550–3650 MHz spectrum measured near San Diego on June 16, 2012.....	51
Figure C-19. M4 statistics of 3550–3650 MHz spectrum measured near San Diego on June 17, 2012.	52
Figure C-20. Spectrogram and band occupancy for 3550–3650 MHz spectrum measured near San Diego on June 17, 2012.....	52
Figure C-21. M4 statistics of 3550–3650 MHz spectrum measured near San Diego on June 18, 2012.	53
Figure C-22. Spectrogram and band occupancy for 3550–3650 MHz spectrum measured near San Diego on June 18, 2012.....	53
Figure C-23. M4 statistics of 3550–3650 MHz spectrum measured near San Diego on June 19, 2012.	54
Figure C-24. Spectrogram and band occupancy for 3550–3650 MHz spectrum measured near San Diego on June 19, 2012.....	54
Figure C-25. M4 statistics of 3550–3650 MHz spectrum measured near San Diego on June 20, 2012.	55
Figure C-26. Spectrogram and band occupancy for 3550–3650 MHz spectrum measured near San Diego on June 20, 2012.....	55

Figure C-27. M4 statistics of 3550–3650 MHz spectrum measured near San Diego on June 21, 2012.	56
Figure C-28. Spectrogram and band occupancy for 3550–3650 MHz spectrum measured near San Diego on June 21, 2012.	56

LIST OF TABLES

Table 1. SPN-43 design parameters [5].	4
Table 2. Radar occupancy measurement system parameters.	6
Table 3. Frequency-swept measurement parameters.	8
Table 4. Time-domain measurement parameters.	9
Table 5. Daily mean band occupancy data.	22
Table 6. Band occupancy statistics for June 8–21, 2012, near San Diego.	22
Table 7. Channel occupancy statistics \hat{p} , c_1 , and c_2 for 90% confidence p and -83 dBm threshold measured in June 2012 near San Diego.	24
Table 8. Mean time intervals ($L = -83$ dBm) measured in June 2012 near San Diego.	28

VARIABLES AND ACRONYMS

$*,*$	Convolution operator
β	Band occupancy
γ_a, γ_e	Earth's actual/effective curvature
Δ	Pulse width
ε	Complimentary confidence interval
λ	Average rate of arrival in a Poisson counting process
ν	Number of successes in a Bernoulli experiment
μs	Microseconds (10^{-6} seconds)
ξ_j, ξ_{jk}	Measured sample function of channel occupancy
τ_j	Time between samples
$\theta_{k\ell}$	Transition probabilities in the steady-state equations for a 1 st order Markov chain
$\Phi(\cdot)$	Cumulative distribution function of the standard normal deviate
ω	Outcome of an experiment
Ω	Set of possible outcomes of an experiment
ASR	Airport Surveillance Radar
ATC	Air Traffic Control
B	Resolution bandwidth in context of spectrum analyzer measurements
B_{eq}	Noise equivalent bandwidth
c	Speed of light
c_1, c_2	Confidence limits
cdf	Cumulative distribution function
d_L	Distance to the edge of the line-of-sight region
dB	Decibel; logarithmic unit used to expressed the ratio between two values
dB _i	Power ratio in decibels relative to isotropic radiator
dB _m	Power ratio in decibels of measured power referenced to one milliwatt

$D(\varepsilon)$	Domain in $p - \hat{p}$ plane that defines confidence intervals
e	Base of the natural logarithm function
$\mathcal{E}\{\cdot\}$	Expected value operator
ENR	Excess Noise Ratio
f	Frequency
$f_{0,k}$	Frequency of the maximum level of the k^{th} signal measured in a FS measurement
$f_{\{V,W,Y\}}$	Probability density function of random variables V , W , or Y
F_n	Noise figure
$F_{\{V,W,Y\}}$	Cumulative distribution function of random variables V , W , or Y
FCC	Federal Communications Commission
FS	Frequency-swept (measurement)
$g(p, \hat{p})$	Joint probability density function of p and \hat{p}
G	Gain (of measurement system in the context of this report)
G_a	Gain of antenna (SPN-43 antenna in the context of this report)
G_R	Gain of receive antenna
G_T	Gain of transmit antenna
GHz	Gigahertz (10^9 hertz)
h_1, h_2	Antenna height above sea level of terminal $\{1, 2\}$
iid	Independent and identically distributed
ISART	International Symposium on Advanced Radio Technologies
ITM	Irregular Terrain Model
ITS	Institute for Telecommunication Sciences
k	Boltzmann's constant or counting variable (depending on context)
L, L_i	Occupancy threshold(s)
$L(r)$	Basic transmission or propagation loss
L_c	Cable loss (of cable between antenna and front end of measurement system)

L_{LOS}	Loss in a LOS scenario governed by free-space propagation loss
L_{pol}	Loss due to polarization mismatch
LNA	Low noise amplifier
LOS	Line of Sight
LTE	Long Term Evolution
M_{β}	Mean band occupancy
M_V	Mean transmission length
M_W	Mean time between transmissions
M_Y	Mean inter-arrival time estimator
MHz	Megahertz (10^6 hertz)
N	Number of measurements or trials
N_c	Number of channels
N_R	Number of renewals
NEXRAD	NEXt generation RADAR
NTIA	National Telecommunications and Information Administration
p	Probability channel is occupied, channel occupancy
\hat{p}	Channel occupancy estimate
P_n	Mean system noise power or RMS-detected system noise
P_{on}, P_{off}	Measured mean power with input signal on/off (Y-factor calibration method)
P_R	Mean power received
P_T	Mean power transmitted
$\wp\{\cdot\}$	Probability operator
$\wp\{\cdot \cdot\}$	Conditional probability operator
pdf	probability density function
q	Probability channel is vacant
$Q_{0,k}$	Maximum signal level of the k^{th} signal in a peak-detected FS measurement

Q_{fs}	Peak-detected power from a frequency-swept peak-measurement
Q_n	Peak-detected system noise power
r	Range
r_{min}, r_{max}	Minimum/Maximum detectable range
RF	Radiofrequency
RMS	Root Mean Square
SA	Spectrum Analyzer
SPN-43	Maritime air-marshaling radar that operates in the upper S-band
t	Time
\mathfrak{T}	Set of possible times
t_d	Dwell time
T	Temperature (Kelvin) or time interval a channel is observed
T_a	Antenna rotation period
T_p	Pulse interval or period
V	Transmission length
$var\{\cdot\}$	Variance operator
W	Time between transmissions
WiMAX	Worldwide Interoperability for Microwave Access
$\mathbf{X}(\mathbf{t}, \boldsymbol{\omega})$	Channel occupancy random process
y	Y factor (Y-factor calibration method)
Y	Renewal time

SPECTRUM OCCUPANCY MEASUREMENTS OF THE 3550–3650 MEGAHERTZ MARITIME RADAR BAND NEAR SAN DIEGO, CALIFORNIA

Michael Cotton and Roger Dalke¹

This report presents spectrum occupancy data of the 3550–3650 megahertz (MHz) maritime radar band measured in June 2012 near San Diego. In this band, the military operates SPN-43 air marshaling radar systems with well-defined signal characteristics. A measurement system and frequency-swept technique were designed specifically to detect SPN-43 emissions. Over the two-week measurement duration in June 2012, we observed multiple systems operating simultaneously in band, spectral spreading of SPN-43 emissions, and out-of-band pulsed emissions that spanned the entire band of interest. In this presumably high-usage mostly military spectrum environment and at a low occupancy threshold (i.e., -83 dBm in a 1 MHz bandwidth at the output of a 2 dBi antenna), mean band occupancy was {36.6, 7.5}% during {weekdays, weekends}. There was a {40.0, 59.8}% chance that the band was empty and a {18.4, 2.3}% chance that the band was full. During weekdays, spectrum usage was dominated by out-of-band pulsed transmissions that spanned the entire band at a relatively low level (approximately 10 dB above the low threshold level). These signals were superimposed on the stronger SPN-43 signals. On average during weekdays, transmissions occurred every four hours with a mean transmission length of approximately 1.5 hours. In contrast, weekend spectrum usage was primarily SPN-43 transmissions at 3.59 GHz arriving every 29 hours (on average) with a mean transmission length of approximately 9 hours. Measured SPN-43 signal amplitudes were at times strong enough to overload the measurement system (exceeding the -83 dBm threshold level by more than 60 dB). Statistical considerations that arise when measured data are used to characterize spectrum occupancy are also discussed in this report. Covered topics include channel occupancy definition, estimation, and uncertainty.

Key words: spectrum occupancy, maritime radar, spectrum management.

1 INTRODUCTION

The purpose of this report is to provide measured occupancy data on systems operating in the 3550–3650 megahertz (MHz) maritime radar band (henceforth called 3.6 GHz band) in support of the development of well-engineered spectrum rules and decisions.

¹ The authors are with the Institute for Telecommunication Science, National Telecommunications and Information Administration, U.S. Department of Commerce, Boulder, CO 80305.

1.1 Background

The 3.6 GHz band was identified as a candidate to accommodate wireless broadband systems in the National Telecommunications and Information Administration (NTIA) 2010 Fast Track Evaluation Report [1] and was a focus of the President's Council of Advisors on Science and Technology (PCAST) 2012 report on realizing the full potential of government-held spectrum to spur economic growth [2]. Radar spectrum management and usage, in general, was also the topic for discussion in the 2011 International Symposium of Advanced Radio Technologies (ISART) [3], hosted by NTIA's Institute for Telecommunication Sciences (ITS) with the purpose of developing forward-thinking rules and processes to fully exploit spectrum resources. More recently, the Federal Communications Commission (FCC) inquired about the possibility of new commercial entrants using the 3.6 GHz band in ways that do not conflict with maritime military operations [4].

Incumbent SPN-43 systems in the 3.6 GHz band are U.S. Navy shipborne mobile installations constrained geographically to U.S. littoral waters and navigable rivers. Spectrum sharing could be coordinated via geographic separation as described by the exclusion zones in [1]. However, over 55% of the U.S. population is concentrated within 50 miles of the coastline [3]. Hence, a spectrum sharing scheme limited to geographic separation via exclusion zones along the coast would exclude large markets, rendering the sharing scenario somewhat unfulfilling. Alternatively and in addition, temporal or dynamic coordination for systems operating inside the exclusion zones has been proposed [2] [3]. Given the importance and mobility of the incumbent systems, successful deployment of this type of dynamic coordination would require large investment to thoroughly evaluate the electromagnetic compatibility between the incumbent and entrant systems, negotiate acceptable conditions for sharing, and develop a sophisticated and secure sharing scheme that satisfies all stakeholders.

Before that level of investment and work can be justified, information about incumbent operations and usage patterns should be assessed. Toward that end, we present in this report spectrum measurements of the 3.6 GHz band performed over two weeks in June 2012 near San Diego, which is presumed to be a relatively high-usage environment given the close proximity to the San Diego Naval base.

1.2 Organization of this Report

In this report, we provide information and results in an increasingly rigorous fashion to develop a framework for measuring and modeling spectrum usage in general and (more specifically) to characterize how military incumbents are currently using this band near San Diego. Section 2 provides SPN-43 system and operational parameters that are required to design an appropriate detection scheme optimized to detect these systems. Section 3 describes the overall measurement methodology, which includes system design and calibration, detection scheme and parameters, data acquisition procedures, and range of detection calculations. Section 4 presents observed signal patterns on a qualitative level for the entire two-week measurement. Data presented in this section include measured calibration data, maximum received signal power and system overload indicators, measurement time resolution, and measured signal levels versus time and frequency.

Next, we develop the theoretical framework to reduce the data to a meaningful set of statistics and estimates with quantified uncertainties. In Section 5 and supported by Appendices A and B, we define channel occupancy in the context of renewal theory. Both channel and band occupancy concepts are developed according to whether or not a received signal level exceeds a pre-specified threshold, which allows for the problems to be modelled as a sequence of 0s and 1s. More specifically, channel occupancy estimation reduces to counting the number of successes in N Bernoulli trials for which many theoretical results are available. We develop estimation of channel occupancy from measurement of limited duration and discuss confidence in the estimate with consideration to dependent versus independent sampling assumptions.

Finally, Section 6 provides quantitative measurement results according to the theory established in Section 5. First, daily mean band occupancy statistics (Section 6.1.1) and plotted results (Appendix C) provide adequate information to develop assumptions on the stationarity in time of the underlying spectrum usage process. Specifically, the results call for a separation of weekday and weekend data, on which we follow through in the remainder of the data processing. Section 6.1.2 provides weekday and weekend band occupancy statistics for the full two-week measurement duration. Section 6.2 provides channel occupancy estimates with 90% confidence intervals versus frequency. Finally, Section 6.3 gives mean transmission interval estimates versus frequency. Section 7 is an overall summary of our findings.

2 SPN-43 SYSTEM DESCRIPTION

It is necessary to understand the signals one aims to measure in order to design the optimal measurement strategy. The frequency band of interest is within the S-band radar spectrum (shown in Figure 1). Major systems that operate in the lower S-band from 2.7 to 2.9 GHz include NEXRAD, airport surveillance radar (ASR), and GPN (where G = ground, P = radar, and N = navigation according to the military naming convention) systems. The upper S-band, ranging from 2.9 to 3.65 GHz, is used for radiolocation; maritime surface search; aerial- and ground-based navigation; air traffic control (ATC); and short-range artillery search, track, and warning.

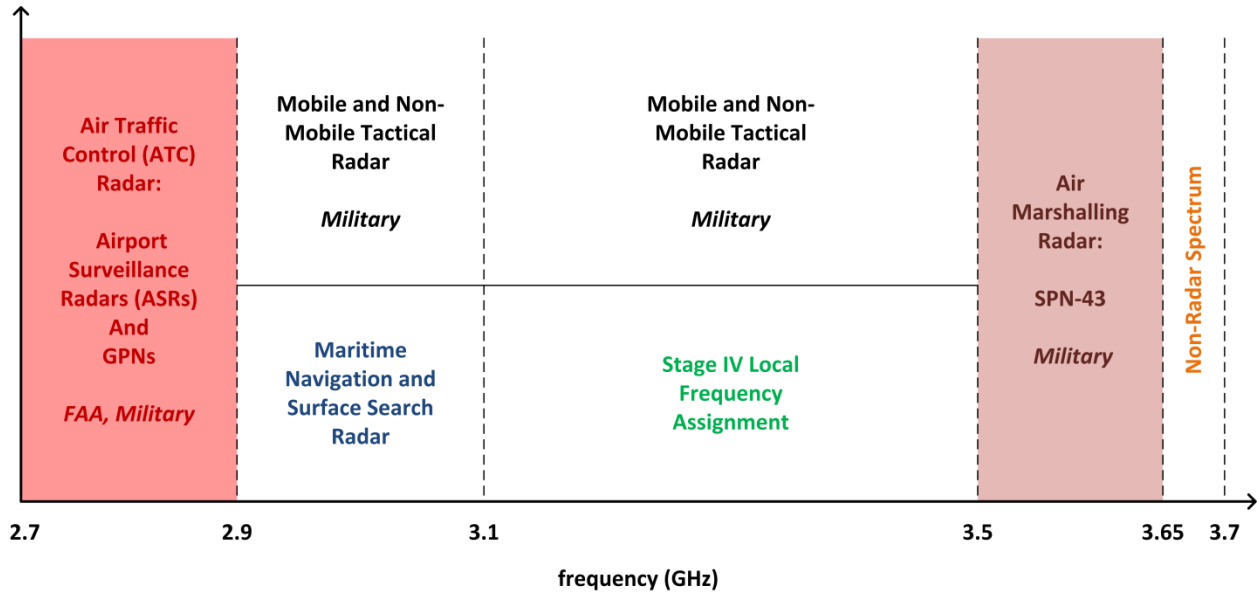


Figure 1. S-Band radar spectrum.

The military operates SPN-43 air marshalling radar systems in a 150 MHz band from 3.5 to 3.65 GHz. SPN-43 radar systems are mobile shipborne radar systems (primarily installed on U.S. Navy Aircraft Carriers), which can be located in all U.S. littoral waters and navigable rivers. SPN-43 transmits high-power pulses through a high-gain antenna that spins azimuthally at a constant rate. Table 1 summarizes SPN-43 design parameters.

Table 1. SPN-43 design parameters [5].

Transmitter	
Tuning Range	3.5-3.65 GHz
Pulse Generation Method	Magnetron
Pulse Interval, T_p	889 (± 20) μ s
Pulse Width, Δ	0.9 (± 0.15) μ s
Power, P_T	850 (± 150) kW
Antenna	
Polarization	Horizontal or circular, switchable
Gain (boresight), G_a	32 dBi
Rotation Period, T_a	4 s

3 MEASUREMENT STRATEGY

San Diego was chosen as the measurement location because of the close proximity to the San Diego Naval base. Point Loma provided a good location for the measurement equipment with a 180 degree field of view over the ocean where ships with the radar travel. The measurements were performed over a course of two weeks in June 2012.

This section provides a full description of the radar occupancy measurement system and procedure. The system was automated and designed to run continuously unless interrupted by the operator. User interaction (e.g., system monitoring, start/stop) occurred via a graphical user interface developed specifically for this measurement. At a high level, the 150 MHz SPN-43 band was divided into 150 one-megahertz channels. This is thought to be a reasonable unit, approximately equal to the reciprocal pulse width of the SPN-43. The measurement system acquired the peak power of each channel and declared the channel occupied if the received peak power exceeded a pre-determined threshold.

3.1 System Description

Figure 2 is a block diagram of the radar occupancy measurement system. Moving from left to right in the RF path, the antenna was a vertically (linear) polarized omnidirectional antenna with 65 degree beamwidth and a nominal gain of $G_R = 2$ dBi at the horizon. Note the polarization mismatch between the SPN-43 (horizontal linear or circular) and the measurement system. This is accounted for with a minimum polarization mismatch factor (L_{pol}), given by manufacturer specification to be $L_{pol} = \{20, 3\}$ dB for {horizontally, circularly} polarized signals.

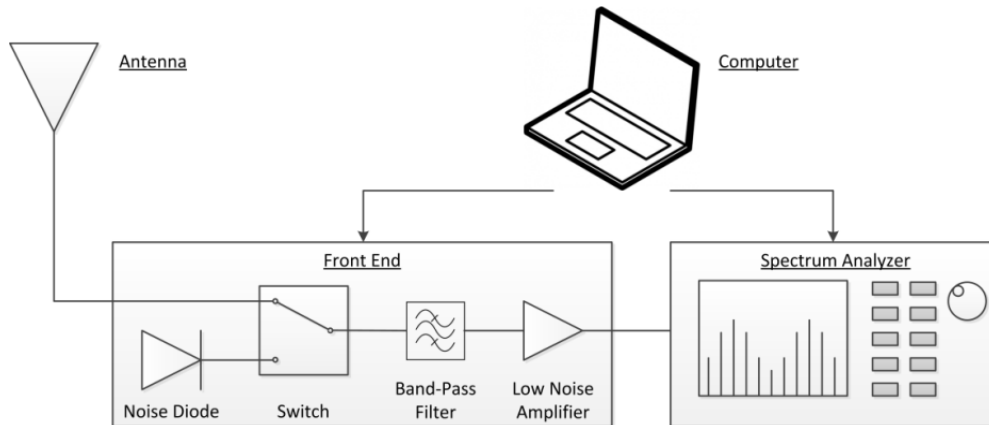


Figure 2. Block diagram of radar occupancy measurement system.

The antenna was connected to one input of an RF switch, which switched between the antenna during occupancy measurements and a noise diode with a 13.7 dB excess noise ratio (ENR) during calibration measurements. The received signal then moved through a 3.5–3.65 GHz band-pass filter, through a low-noise amplifier (LNA), and finally to a spectrum analyzer (SA) that offered frequency-swept (FS) and time-domain peak- and sample-detection measurements. The LNA had 33 dB gain, 5 dB noise figure, and 30 dBm 1 dBm compression point. The LNA gain

improved the sensitivity of the system, which included an SA with a 22 dB noise figure. The high LNA 1 dB compression point ensured that the SA overloaded before the LNA. The switch, power to noise diode, and SA were computer controlled to minimize human error, to allow for automated continuous measurements, and to monitor the system (e.g., for SA overloads.)

Table 2 provides a summary of the radar occupancy measurement system parameters. Regarding overall system parameters, the noise figure was nominally $F_n = 7.5$ dB and system gain was approximately $G = 28$ dB. As indicated in the calibration measurement description (Section 3.2.1), these parameters are referenced to the input of the front end. Dynamic range of the system was from -83 dBm to -22 dBm at the antenna terminal. All power levels provided in this report are referenced to the receive antenna terminal.

Table 2. Radar occupancy measurement system parameters.

Antenna	
Polarization	Vertical
Gain, G_R	2 dBi
Cross-Polarization Loss, L_{pol}	20 dB
Cable Loss, L_c	5 dB
Front End	
Noise Diode – Excess Noise Ratio, ENR	13.7 dB
Band-Pass Filter – Frequency Range	3.5 – 3.65 GHz
Band-Pass Filter – Insertion Loss	1 dB
Low-Noise Amplifier – Gain	33 dB
Low-Noise Amplifier – Noise Figure	5 dB
Low-Noise Amplifier – 1 dB compression	30 dBm
System (front end and SA)	
Gain, G	28 dB
Noise Figure, F_n	7.5 dB

3.2 Measurement Procedure

The computer-controlled measurement system was designed to cycle through a well-defined procedure comprised of the following tasks: (1) hourly system calibration measurements, (2) FS occupancy measurements, and (3) time-domain signal characterization measurements.

3.2.1 System Calibration

System calibration is important for monitoring system integrity and determining minimum occupancy thresholds. Once per hour, F_n and G were measured via the Y-factor method [6]. In this method, the RF switch set the system input to the noise diode, dc power to the noise diode was turned off and the SA measured mean power P_{off} . Next, dc power to the noise diode was turned on and the SA measured mean power P_{on} . The mean power measurements were performed at the center frequency of each of the 150 one-megahertz channels using the SA root mean square (RMS) detector with a 1 MHz resolution bandwidth (B) and a 0.1 second averaging time.

Calibration results were calculated via

$$F_n = \frac{ENR}{(1-y)} \quad \text{and} \quad G = \frac{P_{on}}{kTB_{eq}(ENR + F_n)} , \quad (1)$$

where $y = P_{on}/P_{off}$ is the y-factor and $B_{eq} = 1.128B$ is the noise equivalent bandwidth for the SA utilized in this measurement [7]. F_n and G provide the means to predict RMS- and peak-detected levels of the system noise. The mean noise power at the output of the receive antenna is

$$P_n = kTB_{eq}F_nL_c , \quad (2)$$

where k is Boltzmann's constant, T is temperature in Kelvin, and L_c is loss in the cable that connects the antenna to the front end input.

The expected peak-detected system noise level is a function of dwell time (t_d) and B , i.e.,

$$Q_n(P_n, t_d, B) = P_n \ln[2\pi t_d(1.499B) + e] , \quad (3)$$

where $e \approx 2.71828$ is the base of the natural logarithm function (\ln) [7]. Figure 3 illustrates Q_n/P_n for parameters relevant to this measurement effort. As will be discussed later, $t_d = \{6 \text{ s}, 5 \text{ ms}, 2 \mu\text{s}\}$ for the three different peak-detected measurements performed during the automated measurement procedure. The peak-to-average ratios of the system noise in a 1 MHz bandwidth for these settings are $Q_n/P_n = \{12.5, 10.3, 4.9\}$ dB.

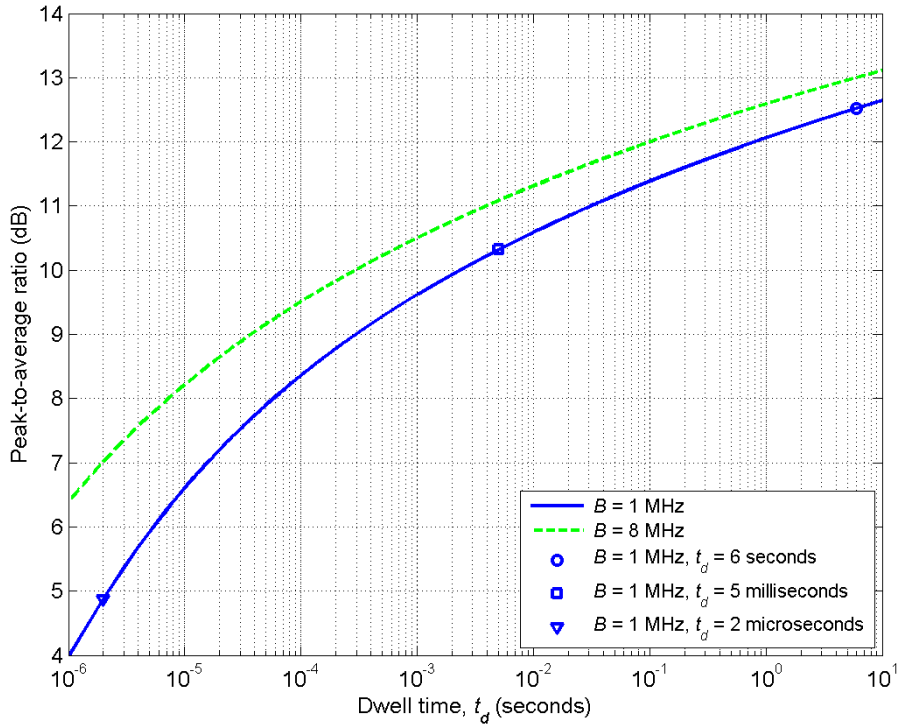


Figure 3. Peak-to-average ratio of complex Gaussian noise versus dwell time and bandwidth.

3.2.2 Frequency-Swept Occupancy Measurements

The core measurement in this effort is the FS occupancy measurement with parameters provided in Table 3. Peak-detected data (Q_{f_s}) was acquired in a 1 MHz resolution bandwidth at each channel across the 150 MHz band. Dwell time was chosen to be $t_d = 1.5T_a = 6$ seconds to ensure that at least one radar antenna rotation period was captured during each channel measurement. Each sweep across the band took 15 minutes. Note that this peak detection scheme eliminates the effect of radar antenna rotation and pulse on/off from the spectrum occupancy calculation.

Table 3. Frequency-swept measurement parameters.

Measurement	Detection	Span (MHz)	Frequency Step (MHz)	B (MHz)	Dwell Time (s)	Sweep Time (s)
Occupancy	Peak	150	1	1	6	900

Figure 4 gives an example FS measurement (blue curve). The horizontal grey band illustrates system noise bounded on the bottom by P_n and on top by Q_n . In this example, there were two signals detected, each spanning a number of 1 MHz channels. The vertical red lines denote the frequency, $f_{0,k}$, of the maximum level for the k^{th} observed signal ($Q_{0,k}$).

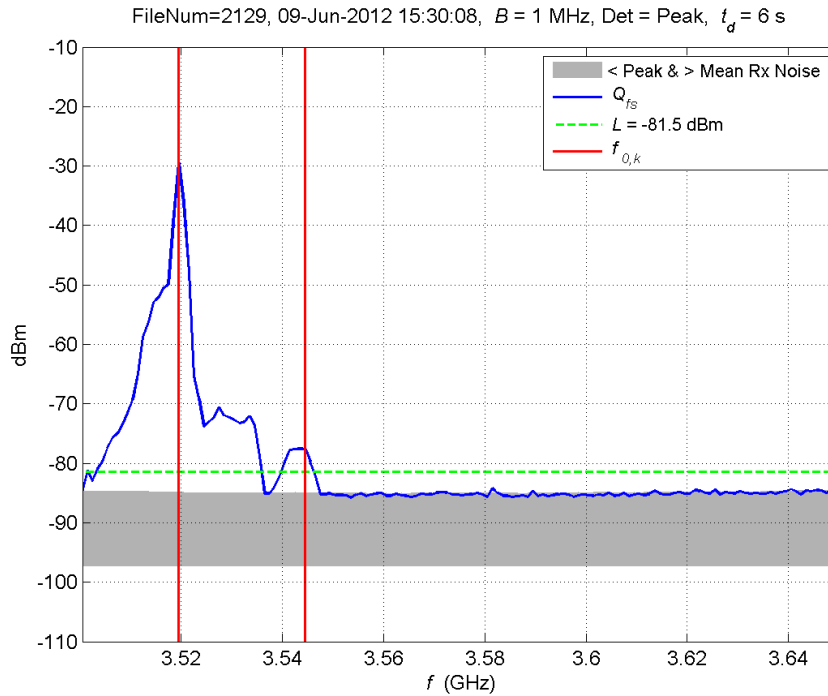


Figure 4. Example frequency-swept occupancy measurement.

The dashed green curve is the occupancy threshold which the control code sets to $L = 2Q_n$ (calculated from the latest calibration measurement.) If we assume that the system noise is a complex Gaussian process, then the amplitude (squared) of the system noise is Rayleigh distributed with an amplitude probability distribution of

$$\wp\{|\mathbf{n}(t)|^2 > z\} = e^{-\frac{z}{P_n}}, \quad (4)$$

where $\wp\{\cdot\}$ is the probability operator. For the given measurement parameters, the probability of system noise power exceeding the threshold, i.e., $\wp\{|\mathbf{n}(t)|^2 > 2Q_n\}$, is on the order of 10^{-16} . From this, it is reasonable to assume that the probability of peak-detected system noise exceeding L is also negligible.

3.2.3 Time-Domain Signal Characterization Measurements

Subsequent to each FS measurement, signal characterization measurements were performed in the time domain at each $f_{0,k}$ to observe SPN-43 antenna rotation period (T_a), pulse interval (T_p), and pulse width (Δ). Time-domain measurements were performed with the SA in zero-span mode and trigger level $Q_{0,k}/4$, i.e., 6 dB below the signal peak. This high trigger level ensured that the time domain measurements were made when the radar antenna was pointing at the measurement system antenna.

Table 4 provides measurement parameters, where time interval is dwell time for peak detection and time between samples for sample detection. SA settings were chosen according to known SPN-43 design parameters to optimize detection and acquire relevant information. Rotation period measurement dwell time was $t_d \cong 5T_p$, which guaranteed that five pulses were available for observation. Pulse interval measurement dwell time was $t_d \cong 2\Delta$ to ensure adequate resolution. Finally, the pulse width measurement sample rate provided approximately 200 samples per pulse width.

Table 4. Time-domain measurement parameters.

Measurement	Detection	B (MHz)	Time Interval (μ s)	Number of Samples
Rotation Period	Peak	1	5000	5000
Pulse Interval	Peak	1	2	5000
Pulse Width	Sample	8	0.005	5000

Figures 5, 6, and 7 give example time-domain signal characterization measurements of the signals at 3.52 GHz and 3.545 GHz. The signal at 3.52 GHz exhibits all the characteristics of a SPN-43 signal, while the signal at 3.545 GHz does not exhibit SPN-43 characteristics.

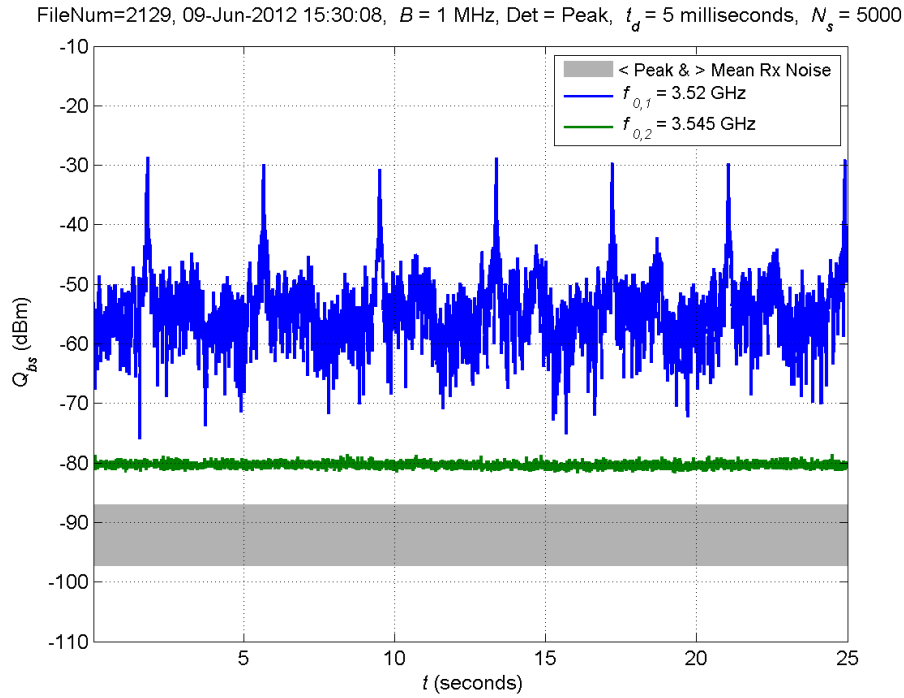


Figure 5. Example rotation period measurement.

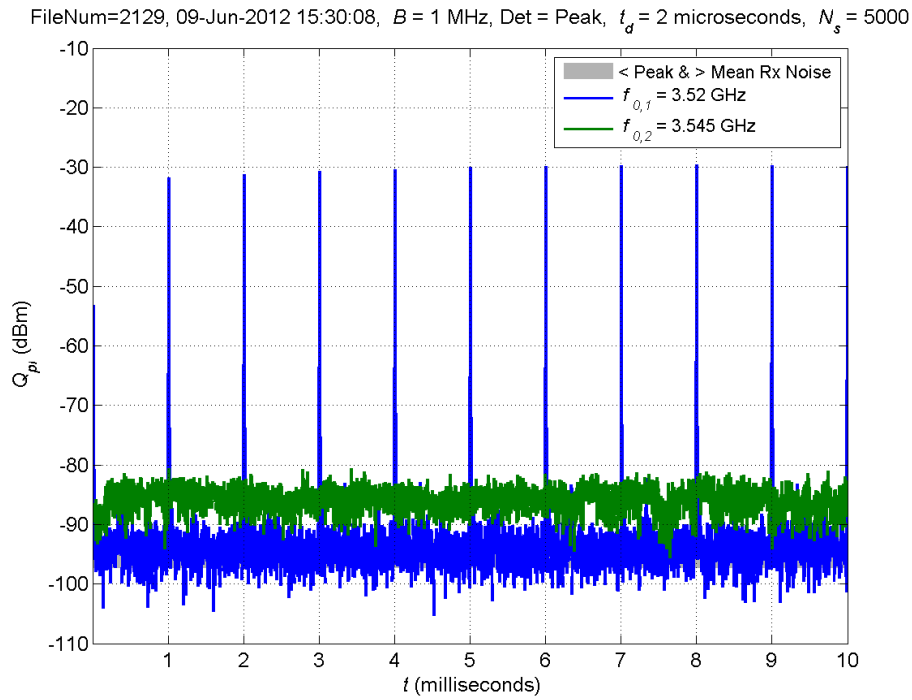


Figure 6. Example pulse-interval measurement.

FileNum=2129, 09-Jun-2012 15:30:08, $B = 8$ MHz, Det = Sample, $\Delta t = 5$ nanoseconds, $N_s = 5000$

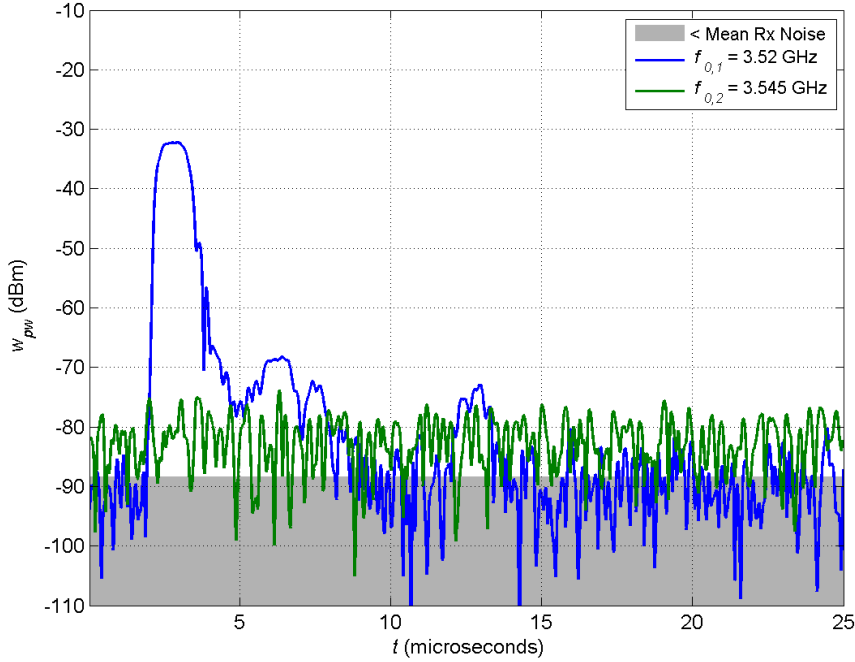


Figure 7. Example pulse-width measurement.

3.3 Range of Detection

In this section, we estimate the maximum detectable range at the occupancy threshold as well as the minimum range without overloading the system. This requires predicting propagation effects over the spherical Earth [8], which can be done with the Irregular Terrain Model (ITM) [9].

When considering long-range propagation over a spherical Earth, there are three range regions characterized by three different propagation mechanisms. Closest to the terminal of interest is the line-of-sight (LOS) region characterized by free-space-loss propagation, i.e.,

$$L_{LOS}(r) = \left(\frac{4\pi r f}{c} \right)^2, \quad (5)$$

where r is range and c is the speed of light. The distance to the edge of the LOS region (d_L) is dependent on antennae heights (h_1, h_2) above sea level. More specifically,

$$d_L = \sqrt{2h_1/\gamma_e} + \sqrt{2h_2/\gamma_e}, \quad (6)$$

where $\gamma_e = \gamma_a(1 - 0.04665e^{N_s/N_1})$ is the Earth's effective curvature, $\gamma_a = 157 \times 10^{-9} \text{ m}^{-1}$ is the Earth's actual curvature, $N_s = 301$ N-units is the minimum monthly mean surface refractivity, and $N_1 = 179.3$ N-units. The region outside LOS is the diffraction region, where loss increases steeply with range. Finally, the troposcatter range is characterized by energy that scatters forward from tropospheric inhomogeneities.

Figure 8 shows ITM results for link geometries relevant to the San Diego spectrum occupancy measurement, where we approximate SPN-43 antenna height above sea level at $h_1 = 50$ m and the ITS measurement antenna height on Point Loma at $h_2 = 140$ m. The left-hand plot displays basic transmission loss versus range for a variety of receiver antenna heights and illustrates the LOS, diffraction, and troposcatter regions. The right-hand plot presents d_L versus h_2 , where $d_L = 78$ km for the San Diego measurement geometry.

Received power can be estimated in linear units as

$$P_R(r) = \frac{P_T G_T G_R}{L_{pol} L(r)}. \quad (7)$$

where $G_T = G_a = 32$ dBi for the current scenario. At the edge of LOS, $L(r) = L_{LOS}(r)$ and received power is predicted to be $\{-38, -21\}$ dBm for $\{\text{horizontal linear, circular}\}$ polarized SPN-43 signals with $L_{pol} = \{20, 3\}$ dB. Working the inverse ITM problem, the minimum propagation loss to avoid overload (i.e., $P_R < -22$ dBm) is $L_{min} = \{125, 142\}$ dB, which translates to approximately $r_{min} = \{12, 72\}$ km from Figure 8. Similarly, the maximum propagation loss that results in the smallest detectable signal (i.e., $P_R > -83$ dBm) is $L_{max} = \{186, 203\}$ dB, which translates to $r_{max} = \{105, 206\}$ km. Hence, the measurement system could detect horizontal polarized SPN-43 systems only 27 km beyond LOS but could detect circular polarized systems well into the troposcatter region.

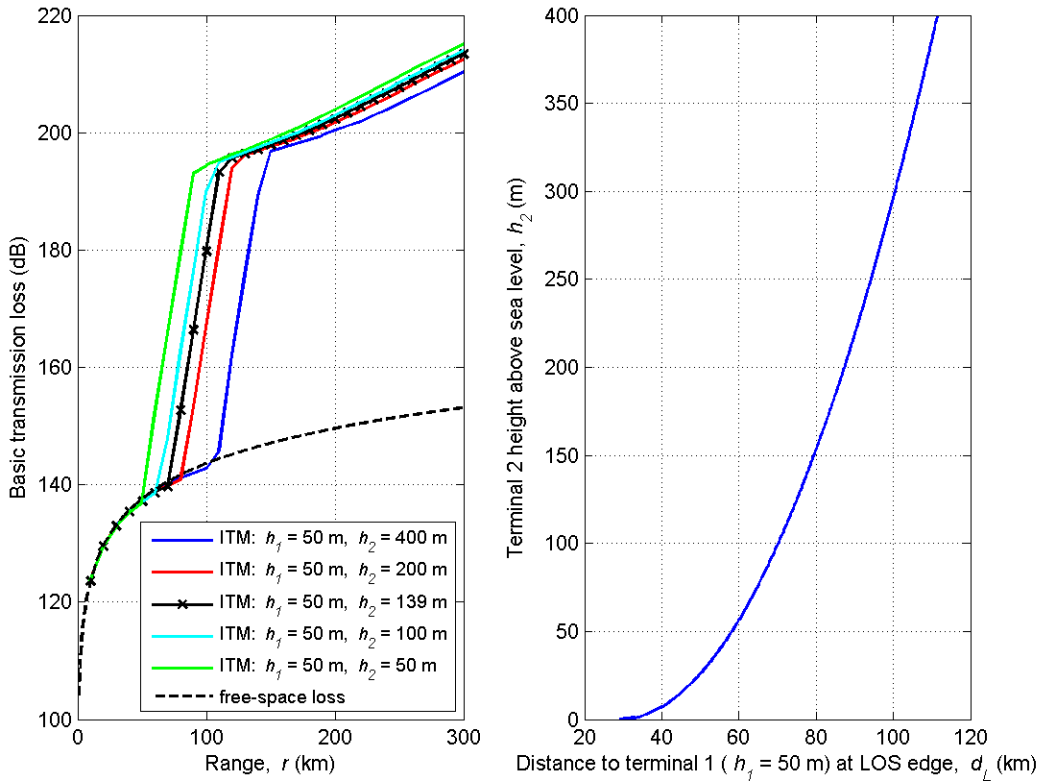


Figure 8. Irregular Terrain Model predictions of basic transmission loss versus range and distance to line-of-sight edge for different terminal heights.

4 OBSERVED SIGNAL PATTERNS

In this section, the patterns of observed signals are demonstrated on a qualitative level. Calibration and maximum received signal power data illustrate system parameters and condition versus time. Next, measurement time resolution is presented. Finally, a spectrogram of the entire FS data set illustrates patterns in spectrum usage over the full two-week measurement duration.

4.1 Calibration Data

Figure 9 provides calibration results during the full course of the measurement campaign. The vertical shaded areas denote measurement downtimes. Downtimes were needed for system validation, code development, and hardware changes. Note that on Monday (6/11) around noon, we changed the amplifier in the front end to one that could tolerate higher power levels. The new amplifier had higher gain and a lower noise figure, which affected the overall system gain and noise figure as illustrated in the top plot.

The bottom graph in Figure 9 illustrates the system dynamic range for the FS measurement, which is bounded by Q_n on the low end and the spectrum analyzer overload level on the high end. Notice that the new amplifier improved the overall sensitivity, but reduced the maximum power the system could tolerate. The lower plot also provides the maximum power level of all channels measured during each FS measurement, i.e., $\max(Q_{fs})$. There were seven overload events over the course of two weeks.

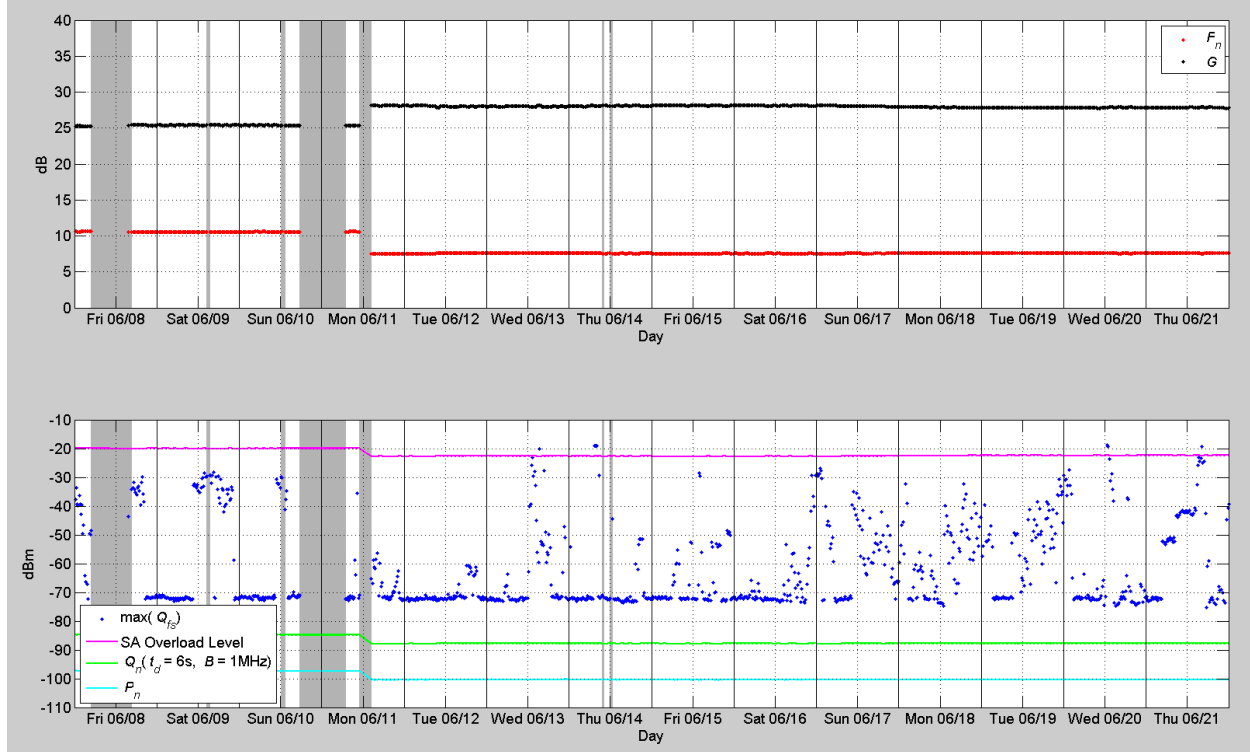


Figure 9. (Top) Calibration data acquired during San Diego measurement and (Bottom) maximum measured power levels compared to system dynamic range.

4.2 Measurement Time Resolution

Time intervals between FS measurements (τ_j) were not constant nor deterministic due to (1) the variable number of time-domain measurements performed (corresponding to the number of $f_{0,k}$ identified in the previous FS measurement) and (2) calibration measurements that occurred on an hourly basis—each of which can occur between any two adjacent FS measurements. Figure 10 illustrates the complimentary cumulative distribution function (cdf) of τ_j for the full data set (measurement downtimes not included). Notice that the probability of $\{\tau_j > 15 \text{ minutes}\}$ is one, which corresponds to the minimum time to sweep through 150 frequencies with a 6 second dwell time. Measurement intervals were as long as 37.3 minutes, and the mean of τ_j was 17.7 minutes.

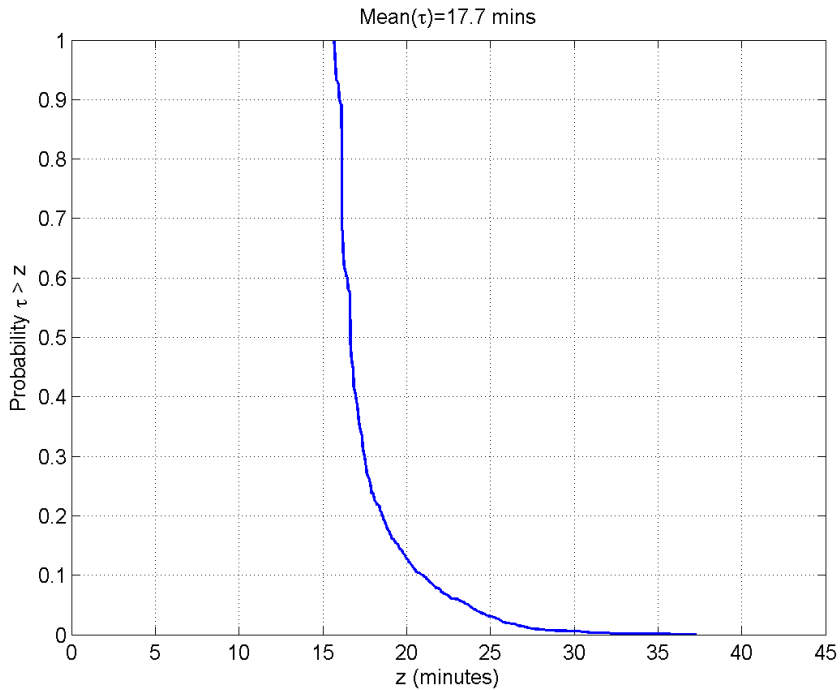


Figure 10. Probability distribution of time between measurements.

4.3 Spectrogram of Full Frequency-Swept Data Set

Figure 11 is a presentation of measured signals for the entire two weeks in San Diego. The middle plot is a spectrogram, where signal level is mapped to color and plotted versus time and frequency. All received signals below -83 dBm are white.

Two signals were continuously present over the entire measurement duration at 3.53 GHz and 3.54 GHz. Figure 11(a) identifies an example of these signals in an FS measurement when no other signals were present. In the time-frequency plot, these signals show up as two thick blue horizontal lines spanning the entire time dimension. In the FCC spectrum license database, these signals correspond to a license to test WiMAX equipment for export markets in the frequency range from 3.4 to 3.6 GHz.

In terms of SPN-43 observations, we observed signals with SPN-43 characteristics at 3.52 and 3.55 GHz (see Figure 11(b) and (c)). Notice the frequency concurrence of these signals with the WiMAX signals. Figure 11(d) shows an SPN-43 signal at 3.59 GHz with a high signal-to-noise ratio. At ISART 2011 [3], we discussed how radar systems commonly operate at power levels outside of the amplifier's linear range, which causes spectral spreading. Notice in this example that spectral spreading caused the SPN-43 signal to exceed occupancy threshold L for all 150 one-megahertz channels from 3.50 to 3.65 GHz. This is also a measurement where the spectrum analyzer was overloaded, as indicated by the red axis. Figure 11(e) illustrates multiple SPN-43 systems operating simultaneously at 3.52, 3.60, and (presumably) 3.61 GHz. Multiple simultaneous SPN-43 signals were common in the last days of the measurements.

Finally, significant out-of-band signals² were observed. Figure 11(f) is a measurement taken three hours after the measurement shown in Figure 11(e). One can observe that the three SPN-43 signals were still present, but there was an additional emission that raised the noise floor across the entire band by about 15 dB. These were out-of-band pulsed signals that turned on and off intermittently over the course of the two weeks. Sometimes, there were high power levels at the lower band edge; other times it was flat across the entire 150 MHz. These out-of-band signals caused many of the vertical blue lines in the time-frequency plot.

² The system's in-band emissions were below 3.5 GHz; out-of-band emissions occurred above 3.5 GHz.

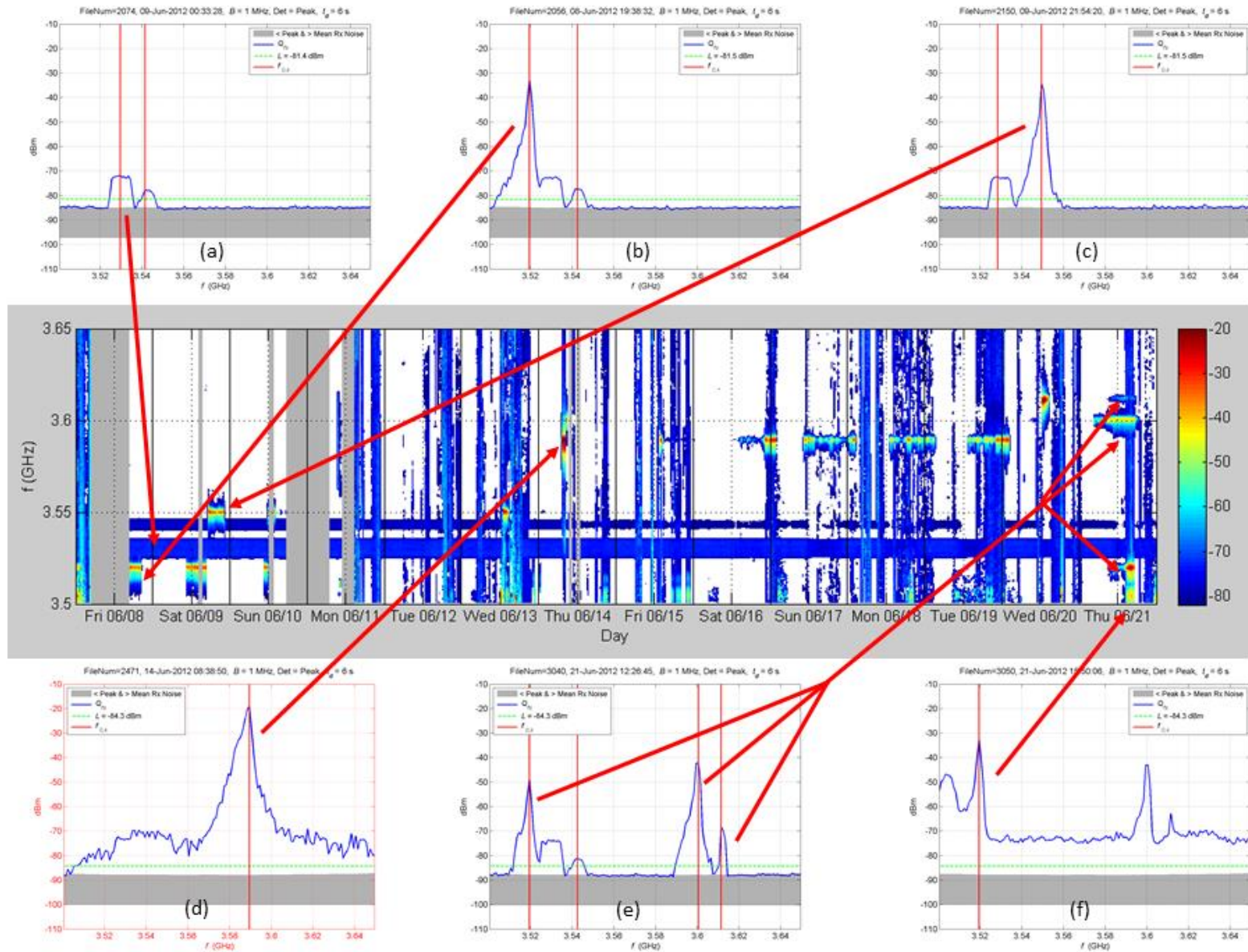


Figure 11. Measured signals in the 3.6 MHz band on June 8–21, 2012, near San Diego.

5 STATISTICAL CONSIDERATIONS FOR SPECTRUM OCCUPANCY MEASUREMENTS

Section 3 provided a measurement and detection strategy specific to the SPN-43 signal characteristics. In this section, we discuss the general definition of channel occupancy as well as means for estimating channel occupancy to a desired level of uncertainty. Further, we consider the aggregate of multiple channels and discuss band occupancy as a metric.

5.1 Renewal Theory and the Definition of Channel Occupancy

Assuming that the received signal power is a random process (which we identify, along with random variables, with bold font), the usual procedure is to define a related two-state random process as follows

$$\mathbf{X}(t) = \begin{cases} 1 & \text{if signal power exceeds threshold } L \\ 0 & \text{else} \end{cases}, \quad (8)$$

and define channel occupancy as

$$p(t) = \wp\{\mathbf{X}(t) = 1\} \quad (9)$$

(see Figure 12 for a depiction of received signal power versus time.) This definition seems satisfactory, i.e., occupancy is equal to the probability that the signal power will exceed a specified level. However, there is a difficulty if $\mathbf{X}(t)$ is some unspecified function of time. In that case, defining a reasonable methodology for measuring occupancy, i.e., estimating $p(t)$, is perhaps not tractable. Hence, we need to make some assumptions about $\mathbf{X}(t)$.

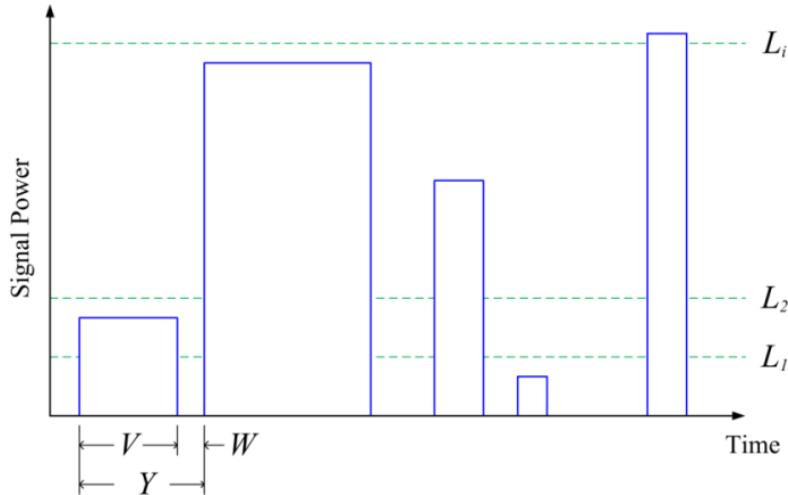


Figure 12. Channel transmissions and related time intervals.

The obvious thing to do is to obtain a realization (i.e., a high fidelity or ideal measurement) of $\mathbf{X}(t)$. From this, we can obtain a series of on-times (\mathbf{V}) and off-times (\mathbf{W}). Note that \mathbf{V} and \mathbf{W} are random variables. In principle, the distributions of these random variables can be accurately estimated from our ideal measurement. We will assume that \mathbf{V} and \mathbf{W} are independent and their

statistics are the same during other similar time periods (e.g., daytime on a weekday). From this measurement, it would seem obvious that occupancy is equal to the fraction of time that the measurement exceeds the specified level. But how does this relate to our original definition of occupancy? For the answer, we look to the theory of renewal processes.

A two-state random process, such as the one described above, with independent on and off times is a renewal process. For such a process, $p(t)$ satisfies the renewal equation [10]

$$p(t) = \wp\{\mathbf{V} > t\} + \int_0^t p(t-y) dF_Y(y) , \quad (10)$$

where F_Y is the cdf of the recurrence time $\mathbf{Y} = \mathbf{V} + \mathbf{W}$.

Furthermore, there are limit theorems that show that as time goes on, $p(t)$ tends to a constant, and in our particular case

$$\lim_{t \rightarrow \infty} p(t) = \frac{\mathcal{E}\{\mathbf{V}\}}{\mathcal{E}\{\mathbf{Y}\}} \quad (11)$$

(see Appendix A for the development of this theorem from first principles). This is good news, because it tells us that our original definition of occupancy tends to the estimate that we would obtain from an ideal measurement. Perhaps more importantly, it tells us that we do not need to accurately measure the statistics of \mathbf{V} and \mathbf{W} , which would significantly tax our resources. All we need to do is estimate $\wp\{\mathbf{X}(t) = 1\}$ from measurement samples. In fact, if the samples are independent, we have a Bernoulli process that can be used to estimate $p(t)$ to the desired level of uncertainty (see Section B.1). Similarly, if the samples are dependent, a Markov process can be used to estimate $p(t)$ to the desired level of uncertainty (see Section B.2).

5.2 Estimation of Channel Occupancy

In general, to estimate channel occupancy, we make N observations of random process $\mathbf{X}(t)$ over time interval T and calculate the time average

$$\hat{p} = \frac{1}{N} \sum_{j=1}^N \xi_j = \frac{\nu}{N} , \quad (12)$$

where ξ_j are the observations and ν is the number of successes. Uncertainty of the estimate is established with the expression

$$\wp\{c_1(\hat{p}) < \mathbf{p} < c_2(\hat{p})\} = 1 - \varepsilon , \quad (13)$$

which states that the actual channel occupancy \mathbf{p} lies within confidence interval (c_1, c_2) with probability $1 - \varepsilon$. Appendix B develops expressions for c_1 and c_2 from first principles under independent and dependent sampling assumptions.

As indicated by the measurement results in the following section, our sampling interval is less than a typical SPN-43 transmission length; hence, dependent sampling is a better assumption. Confidence limits for dependent sampling are given as

$$c_{2,1}(\hat{p}) = \frac{\hat{p} + \frac{\alpha z_\varepsilon^2}{2N} \pm z_\varepsilon \sqrt{\left(\frac{\alpha z_\varepsilon}{2N}\right)^2 + \frac{\alpha \hat{p} \hat{q}}{N}}}{1 + \frac{\alpha z_\varepsilon^2}{N}}, \quad (14)$$

where $\hat{q} = 1 - \hat{p}$. The variable $\alpha = 2\hat{q}/(1 - \hat{\theta}_{11}) - 1$ was introduced in the derivation to simplify the math. It is dependent on the estimate of transition probability θ_{11} , which can be achieved from data via

$$\hat{\theta}_{11} = \frac{1}{\nu - 1} \sum_{j=2}^N \xi_{j-1} \xi_j. \quad (15)$$

Finally, z_ε is the parameter that adjusts the confidence limits according to the desired confidence level. It is calculated for a specified ε via $\varepsilon = 2\Phi(z_\varepsilon)$, where $\Phi(\zeta) = \frac{1}{\sqrt{2\pi}} \int_{-\infty}^{\zeta} e^{-z^2/2} dz$ is the cdf of the standard normal deviate. Solutions to this integral equation are accessible via look up table or the complementary error function, i.e., $\Phi(\zeta) = \frac{1}{2} \operatorname{erfc}\left(\frac{\zeta}{\sqrt{2}}\right)$.

5.3 Estimation of Band Occupancy

A useful metric in the context of FS spectrum occupancy measurements is band occupancy, which is intuitively defined at any given time as the fraction of frequencies (or channels) with a detected signal level that exceeds a predetermined threshold. Then measured band occupancy at a given time is given by

$$\beta_j = \frac{1}{N_c} \sum_{k=1}^{N_c} \xi_{jk}, \quad (16)$$

where ξ_{jk} is the channel observation, j is the time index, k is the channel index, and N_c is the number of channels sampled. Further, we acquire N measurements over time duration T when spectrum usage in the band is assumed to be stationary and acquire the mean band occupancy as

$$M_\beta = \frac{1}{N} \sum_{j=1}^N \beta_j = \frac{1}{N_c} \sum_{k=1}^{N_c} \hat{p}_k, \quad (17)$$

where \hat{p}_k is the channel occupancy estimate for channel k given in (12).

Given that military spectrum usage is based on coordinated frequency assignments, it is not expected that the discrete random process ξ_{jk} would be stationary in frequency. More

specifically, we expect higher mean channel occupancy at assignment center frequencies and lower usage at frequencies between assignments that are kept relatively quiet in order to avoid interference between frequency-adjacent systems. A further complication is that individual channels are not independent due to the fact that the observed signals occupy a number of adjacent channels (defined by our measurement scheme to be 1 MHz). Consequently, since we are accumulating Bernoulli trials from different populations (i.e., from different channels), we do not pursue an uncertainty analysis on the mean band occupancy statistic.

6 MEASUREMENT RESULTS

In this section, band and channel occupancy statistics are provided according to the theoretical framework established previously. Frequency range is limited to 3.55–3.65 GHz, which corresponds to the frequency band specified in the NTIA Fast Track Report [1]. Note that this removes contributions of the WiMAX signals (3.53 and 3.54 GHz) from the occupancy results.

6.1 Band Occupancy

For band occupancy results, threshold levels $L_i = \{-83, -80, -77, -74, -71\}$ dBm are applied to the entire data set. This is in contrast to those used during measurements, where $L = 2Q_n$ was set according to the latest calibration measurement. At the largest measured system noise level, $Q_n = -83.8$ dBm, the probability of system noise exceeding the lowest threshold, $L_1 = -83$ dBm, is calculated from (4) to be on the order of 10^{-10} , which we consider to be negligible.

6.1.1 Daily Means

Band occupancy results provide a coarse view of the data and allow for assumptions to be developed about stationarity in time. Table 5 provides daily mean band occupancy numbers with the number of FS measurements performed on that day. For subsequent discussions, we assume ξ_{jk} is not stationary in general (as observed in Table 5 by the significant differences in weekday versus weekend band occupancy). We do assume, however, that ξ_{jk} is stationary in time on a daily basis if the time duration is limited to weekdays only or weekend days only. This provides some justification for separated weekday and weekend occupancy statistics, which we carry through in the remainder of this report. Given that the full measurement duration is only two weeks, we combine all weekday data together and all weekend data together. If the measurement duration were longer or even continuous, however, we would likely provide weekly statistics for weekday and weekend data.

Appendix B accompanies this data and provides plots of daily band occupancy results and signal levels. Band occupancy data are plotted versus time along with hourly means. Signal levels are in the time versus frequency spectrogram format. Also, maximum, mean, median, and minimum (M4) signal level statistics over a 24 hour period versus frequency are shown. M4 statistics are good for visualizing signal patterns versus frequency over a specified period of time.

Table 5. Daily mean band occupancy data.

Date	N	M_β (%)				
		$L = -83$ dBm	$L = -80$ dBm	$L = -77$ dBm	$L = -74$ dBm	$L = -71$ dBm
Fri 06/08	45	37	35	32	27	21
Sat 06/09	86	2	1	1	1	1
Sun 06/10	63	1	1	0	0	0
Mon 06/11	49	38	35	31	21	9
Tue 06/12	83	31	21	12	9	6
Wed 06/13	84	44	34	25	17	11
Thu 06/14	82	19	12	5	3	2
Fri 06/15	85	32	24	12	6	4
Sat 06/16	82	5	3	2	1	1
Sun 06/17	75	22	16	12	8	4
Mon 06/18	78	56	42	28	18	12
Tue 06/19	77	46	36	25	13	5
Wed 06/20	78	37	30	21	13	6
Thu 06/21	77	28	23	18	12	6

6.1.2 Two-Week Statistics

Under the assumption that weekday spectrum usage is one stationary random process and weekend spectrum usage is another stationary random process, we accumulate weekday and weekend realizations of band occupancy over the full two week measurement duration and plot the complementary cdfs (see Figures 13 and 14). At the left hand side of the plots, observe that the curves do not go to one. In the case of the weekday $L = -83$ dBm threshold (blue curve), $\wp\{\beta_j > 0\% \} \cong 0.6$, which means that there is a 0.40 probability that the band is empty, i.e., $\wp\{\beta_j = 0\% \} \cong 0.4$. Similarly, one can deduce from the right side of the blue curve that the band is completely occupied with probability $\wp\{\beta_j = 100\% \} \cong 0.18$. Table 6 provides a summary of two-week band occupancy statistics.

Table 6. Band occupancy statistics for June 8–21, 2012, near San Diego.

Category	N	L (dBm)	M_β (%)	$\wp\{\beta_j = 0\% \}$ (%)	$\wp\{\beta_j = 100\% \}$ (%)
Weekday	738	-71	7.5	64.8	0.7
		-74	13.0	60.0	1.6
		-77	19.7	50.8	4.5
		-80	28.5	45.7	9.8
		-83	36.6	40.0	18.4
Weekend	306	-71	1.6	69.6	0.0
		-74	2.5	67.7	0.0
		-77	3.9	66.3	0.7
		-80	5.3	63.4	1.6
		-83	7.5	59.8	2.3

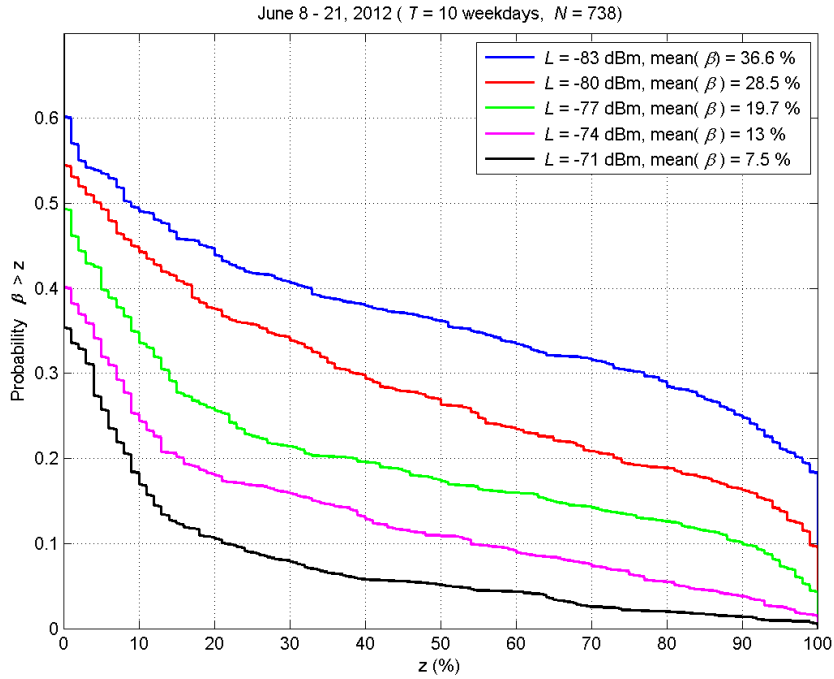


Figure 13. Probability distributions of band occupancy measured during weekdays on June 8–21, 2012, near San Diego.

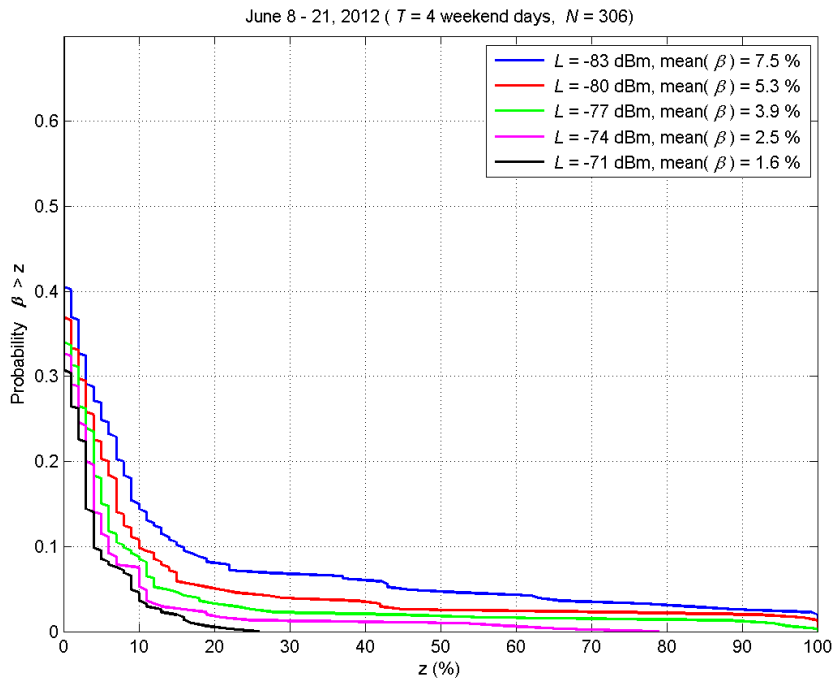


Figure 14. Probability distributions of band occupancy measured during weekends on June 8–21, 2012, near San Diego.

6.2 Channel Occupancy

Channel occupancy results allow for observation of spectrum usage versus frequency. We narrow the scope in this subsection to statistics for the $L = -83$ dBm threshold.

6.2.1 Example Calculations

Before presenting data for each measured channel across the band, we give example calculations for individual cases to make data interpretation more straightforward. Table 7 presents measured channel occupancy statistics for six channels spaced evenly across the band. In the discussion that follows, we focus on the 3.59 GHz and 3.57 GHz channels.

Table 7. Channel occupancy statistics \hat{p} , c_1 , and c_2 for 90% confidence p and -83 dBm threshold measured in June 2012 near San Diego.

Category	N	f (GHz)	N_R	$\hat{\theta}_{11}$ (%)	\hat{p} (%)	c_1 (%)	c_2 (%)
Weekday	738	3.55	53	81.5	39.0	33.1	47.0
		3.57	56	79.8	38.4	32.7	45.9
		3.59	44	86.3	43.6	37.0	52.9
		3.61	69	72.2	33.7	28.9	40.0
		3.63	52	79.7	34.8	29.2	42.5
		3.65	53	77.9	32.7	27.2	40.0
Weekend	306	3.55	9	77.3	15.0	9.4	26.4
		3.57	10	47.4	6.2	3.6	11.1
		3.59	3	96.4	27.5	21.5	68.4
		3.61	5	58.3	3.9	1.8	9.2
		3.63	5	64.3	4.6	2.1	10.9
		3.65	4	73.3	4.9	2.2	13.0

First, consider the channel at 3.59 GHz over the full two week measurement duration. This channel (shaded in red in Table 7) is of interest because it had relatively high channel occupancy due to SPN-43 transmissions. The weekday data is comprised of $N = 738$ trials of which $\nu = 322$ exceeded $L = -83$ dBm for a channel occupancy estimate of $\hat{p} = 43.6\%$. The probability of the channel being occupied given it was occupied on the previous measurement was relatively high, i.e., $\hat{\theta}_{11} = 86.3\%$, which justifies using the dependent sampling model for calculating confidence intervals for \hat{p} . For 90% confidence level, $\varepsilon = 0.1$ and $z_\varepsilon = 1.64$. Substitution into (14) gives confidence limits $c_1 = 37.0\%$ and $c_2 = 52.9\%$.

Weekend data for the same frequency were comprised of $N = 306$ measurements and $\nu = 84$ successes for a channel occupancy estimate of $\hat{p} = 27.5\%$. There were only $N_R = 3$ renewals and the highest dependence between samples, e.g., $\hat{\theta}_{11} = 96.4\%$, which indicates that the transmission stayed on for a relatively long time. The relatively small probability of success, high transition probability (correlation between samples), and small N resulted in increased confidence limits $c_1 = 26.4\%$ and $c_2 = 68.4\%$.

Next, we consider the 3.57 GHz channel, which is of interest because it is 20 MHz away from the nearest SPN-43 center frequency that we observed; hence, occupancy appears to be strongly

influenced by spectral spreading and out-of-band contributions. Consider the weekday data where $\nu = 283$ successes, for a channel occupancy estimate of $\hat{p} = 38.4\%$. There were fewer correlated samples as indicated by a reduced transition probability, i.e., $\hat{\theta}_{11} = 79.8\%$, which resulted in smaller confidence intervals with limits $c_1 = 32.7\%$ and $c_2 = 45.9\%$.

The 3.57 GHz weekend data provide a large number of renewals, i.e., $N_R = 10$, when considering the low channel occupancy estimate, $\hat{p} = 6.2\%$. The measured transition probability is indicative of independent sampling, i.e., $\hat{\theta}_{11} = 47.3\%$, and a relatively small confidence intervals with limits $c_1 = 3.6\%$ and $c_2 = 11.1\%$.

6.2.2 Channel Occupancy Statistics versus Frequency

Figures 15 and 16 illustrate $\hat{\theta}_{11}$ and $\hat{p} \pm c_{1,2}$ versus frequency. Figure 17 illustrates \hat{p} versus frequency for $L_i = \{-83, -80, -77, -74, -71\}$ dBm. For each of these figures, calculations were performed separately for data acquired during weekdays (shown in top plots) and weekends (shown in bottom plots).

Weekday channel occupancy statistics were relatively flat across the band; this is because the out-of-band signals contributed significantly across the band during weekdays. During the 10 weekdays when measurements occurred, there were 5–7 renewals per day (on average) which resulted in mean renewal times ranging from 3 to 5 hours. Channel occupancy across the band was in the range $0.32 < \hat{p} \leq 0.44$. As the occupancy threshold increases (i.e., L increases from -83 dBm to -71 dBm in Figure 17), channel occupancy decreases somewhat uniformly across the band.

In contrast, weekend channel occupancy statistics were more frequency dependent; this is because out-of-band signals did not have significant contributions during the weekends. Channels near 3.59 GHz and 3.55 GHz, where SPN-43 signals were observed, showed elevated levels of $\hat{\theta}_{11}$ and \hat{p} . Note that dependent sampling is a questionable assumption for channels that are quiet during the weekend, as indicated by channels with $\hat{\theta}_{11} \approx 0.5$.

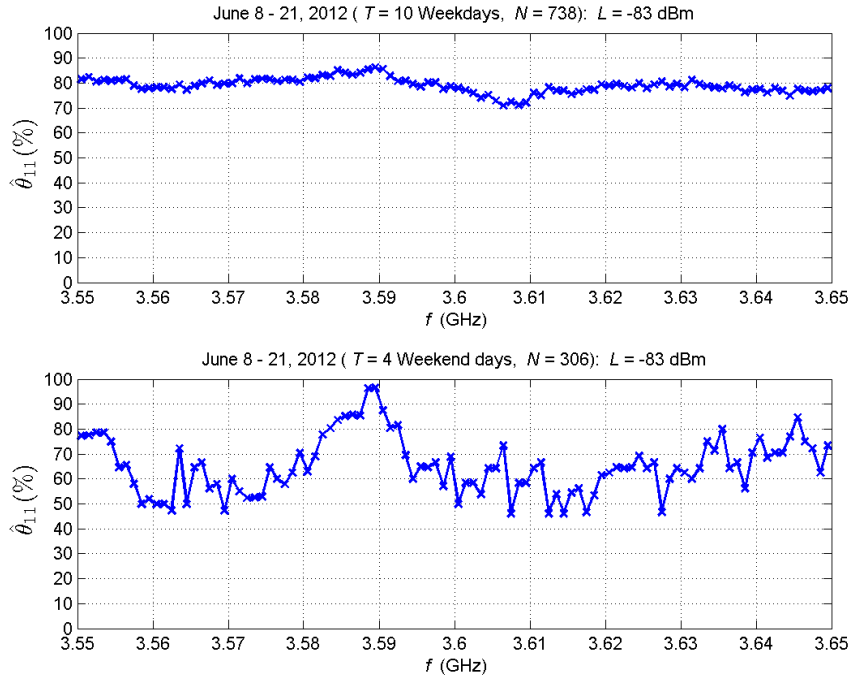


Figure 15. Transition probability ($L = -83$ dBm) versus frequency on June 8–21, 2012, near San Diego.

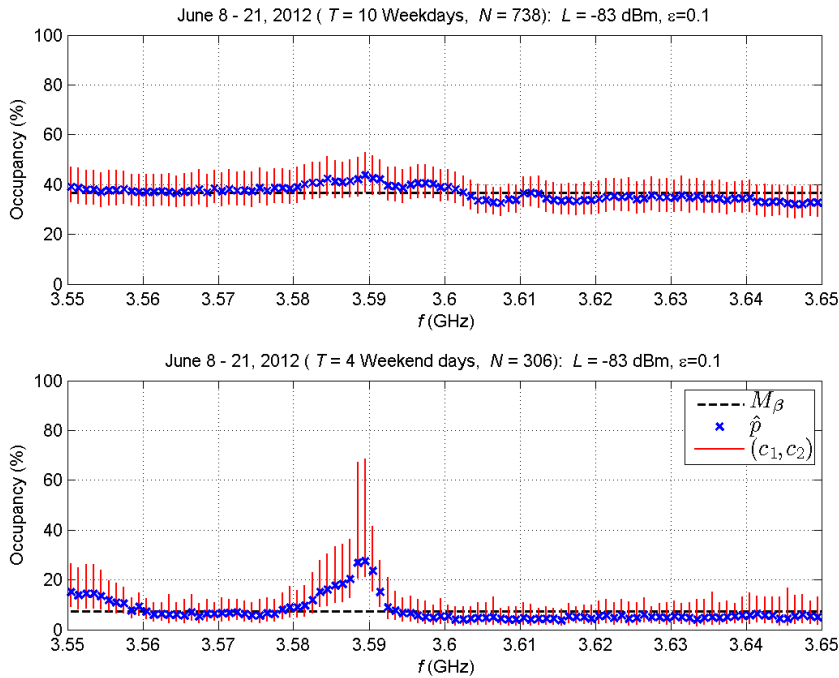


Figure 16. Channel occupancy estimates ($L = -83$ dBm) with 90% confidence intervals versus frequency on June 8–21, 2012, near San Diego.

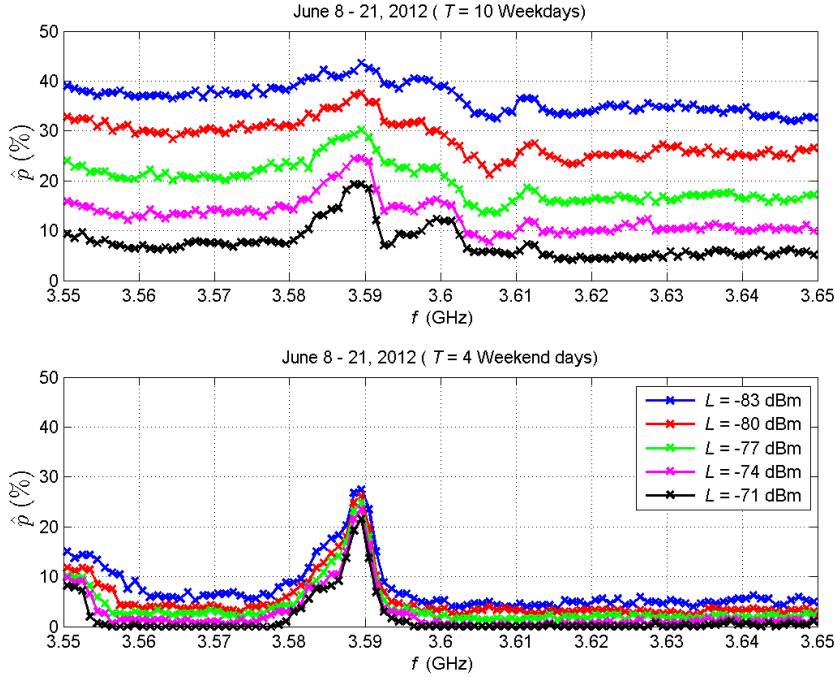


Figure 17. Channel occupancy estimates versus frequency at various threshold levels on June 8–21, 2012, near San Diego.

6.3 Time Intervals

As discussed in Section 5.1 measuring time intervals is a challenging task where accuracy is related to the time resolution of the measurement. Consider the 15 minute minimum time resolution of the measurement strategy described in this report, which would cause difficulties when measuring relatively short transmission lengths. If the mean transmission length were one minute, for example, there could easily be 5 transmissions lost in between samples. In a less severe scenario, if the mean transmission length were one hour, then measured values would be the expected value (one hour) plus or minus 15 minutes.

With these caveats, we also estimated time intervals \mathbf{V} , \mathbf{W} , and \mathbf{Y} to obtain qualitative information on the temporal characteristics of the channel. This information can be valuable in scenarios where coordinated or opportunistic spectrum sharing is considered for improving spectrum utilization.

Estimates of the expected values for \mathbf{V} , \mathbf{W} , and \mathbf{Y} are calculated as

$$M_{\{\mathbf{V}, \mathbf{W}, \mathbf{Y}\}} = \frac{1}{N_R} \sum_{m=1}^{N_R} \{V_m, W_m, Y_m\} , \quad (18)$$

where N_R is the number of renewals and $\{V_m, W_m, Y_m\}$ are realizations of $\{\mathbf{V}, \mathbf{W}, \mathbf{Y}\}$.

Table 8 provides measured mean time intervals for the limited set of channels discussed in Section 6.2.1 and Figure 18 illustrates the measured time intervals for all channels. Note that the weekend 3.59 GHz channel had a mean transmission lengths (M_V) of 8.9 hours due to SPN-43 transmissions (largely in the absence of out-of-band signals). The other channels which were primarily influenced by out-of-band emissions during the weekdays had mean transmission lengths of 1–2 hours.

Table 8. Mean time intervals ($L = -83$ dBm) measured in June 2012 near San Diego.

Category	N	f (GHz)	N_R	M_Y (hours)	M_V (hours)	M_W (hours)
Weekday	738	3.55	53	4.1	1.6	2.5
		3.57	56	3.9	1.5	2.4
		3.59	44	4.9	2.2	2.7
		3.61	69	3.1	1.0	2.1
		3.63	52	4.2	1.4	2.7
		3.65	53	4.1	1.3	2.7
Weekend	306	3.55	9	9.8	1.5	8.3
		3.57	10	8.8	0.6	8.1
		3.59	3	29.3	8.9	20.4
		3.61	5	17.6	0.7	16.8
		3.63	5	17.6	0.8	16.7
		3.65	4	22.0	1.2	20.8

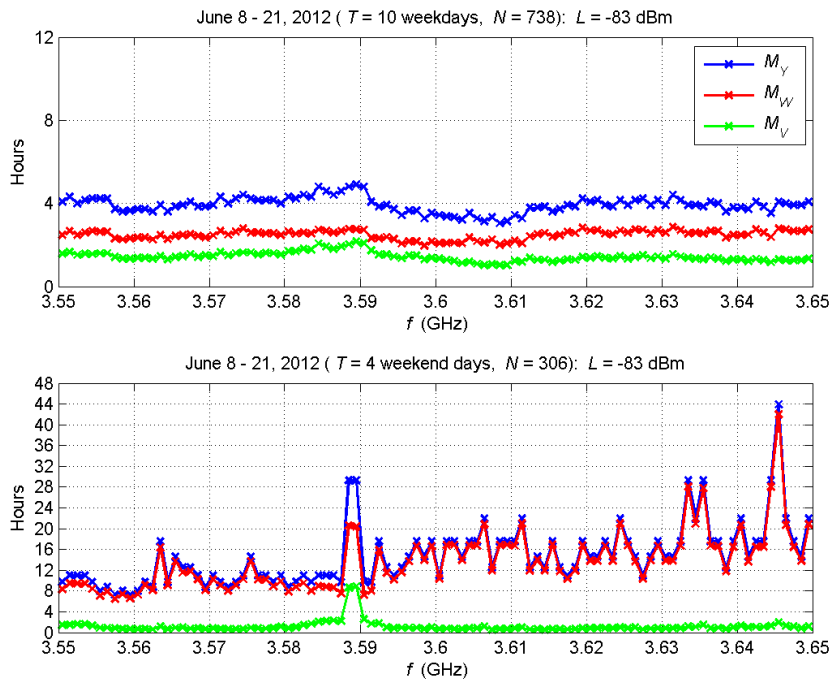


Figure 18. Measured mean transmission intervals ($L = -83$ dBm) versus frequency on June 8–21, 2012, near San Diego.

Figures 19 and 20 present measured complementary cdfs of \mathbf{V} , \mathbf{W} , and \mathbf{Y} for the weekday 3.59 GHz and 3.57 GHz channels, respectively. There were not enough renewal events measured during weekends to warrant distribution plots. For comparison, exponential distribution curves with rate parameters equal to the appropriate reciprocal mean transmission interval are also shown. Mathematically, the exponential complementary cdf is given by $\Pr\{\mathbf{Y} > y\} = \exp(-\lambda y)$.

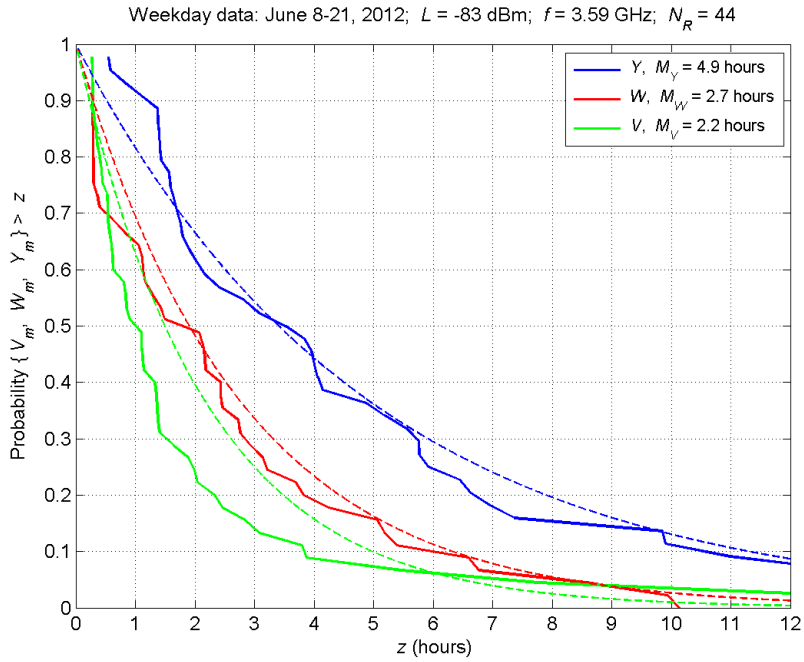


Figure 19. Probability distributions of transmission intervals ($f = 3.59$ GHz, $L = -83$ dBm) measured during weekdays on June 8–21, 2012, near San Diego. Dashed lines are corresponding exponential distributions.

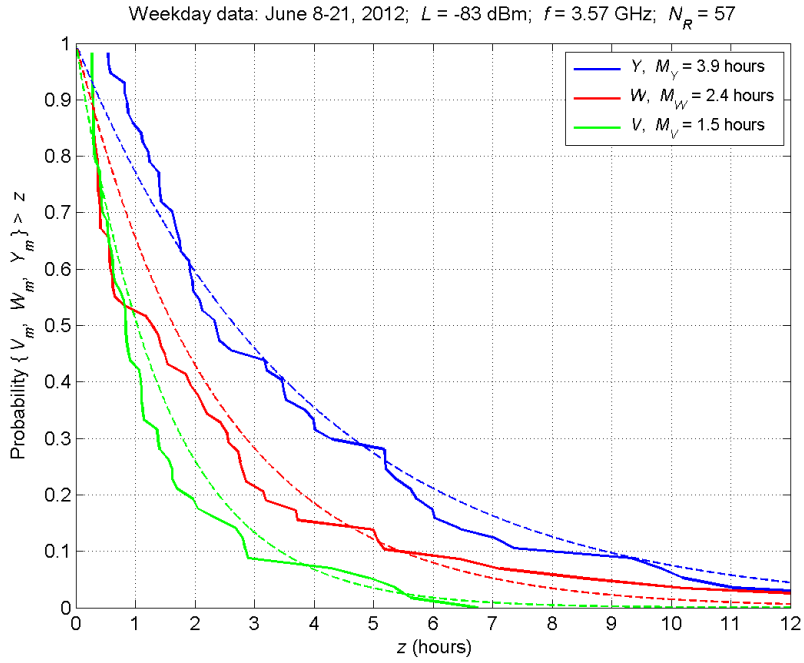


Figure 20. Probability distributions of transmission intervals ($f = 3.57$ GHz, $L = -83$ dBm) measured during weekdays on June 8–21, 2012, near San Diego. Dashed lines are corresponding exponential distributions.

7 SUMMARY

A measurement technique optimized to detect SPN-43 maritime radar signals was described. Further, statistical considerations that arise when measured data are used to characterize spectrum occupancy were discussed. Specifically, a theoretical framework modeling spectrum usage as a renewal process and measuring channel occupancy to a specified level of confidence were established.

The measurement technique was implemented and deployed to measure spectrum occupancy in the 3.6 MHz band for two weeks in June 2012 near San Diego. In this presumably high-usage mostly military spectrum environment and at a low occupancy threshold (i.e., -83 dBm in a 1 MHz bandwidth), mean band occupancy was {36.6, 7.5}% during {weekdays, weekends}. There was a {40.0, 59.8}% chance that the band was empty and a {18.4, 2.3}% chance that the band was full. During weekdays, spectrum usage was dominated by out-of-band pulsed transmissions superimposed on the stronger SPN-43 signals that spanned the entire band at a relatively low level (approximately 10 dB above the low threshold level). On average during weekdays, transmissions arrived every four hours with a mean transmission length of approximately 1.5 hours. In contrast, weekend spectrum usage was primarily SPN-43 transmissions with amplitudes strong enough to overload the measurement system (sometimes exceeding the low threshold level by more than 60 dB). On average during weekends, transmissions (at 3.59 GHz) arrived every 29 hours with a mean transmission length of approximately 9 hours.

8 REFERENCES

- [1] National Telecommunications and Information Administration, “[An Assessment of the Near-Term Viability of Accommodating Wireless Broadband Systems in the 1675–1710 MHz, 1755–1780 MHz, 3500–3650 MHz, and 4200–4220 MHz, 4380–4400 MHz Bands](#),” *NTIA Report*, Oct. 2010.
- [2] President’s Council of Advisors on Science and Technology, “[Realizing the Full Potential of Government-Held Spectrum to Spur Economic Growth](#),” *OSTP/PCAST Report to the President*, Mar. 2012.
- [3] M. Cotton, M. Maior, F. Sanders, E. Nelson, D. Sicker, “[ISART 2011 Proceedings – Developing Forward Thinking Rules and Processes to fully Exploit Spectrum Resources: An Evaluation of Radar Spectrum Usage and Management](#),” *NTIA Special Publication SP-12-485*, Mar. 2012.
- [4] Federal Communications Commission, “[Amendment of the Commission’s Rules with Regard to Commercial Operations in the 3550–3650 MHz Band](#),” *FCC 12-148*, Dec. 2012.
- [5] Department of Defense, “Military Standardization Handbook,” *MIL-HDBK-162B*, Dec. 1973.
- [6] Agilent, “[Noise Figure Measurements Accuracy – The Y-Factor Method](#),” *Application Note 57-2*, May 2010.
- [7] Agilent, “[Spectrum and Signal Analyzer Measurements and Noise](#),” *Application Note*, May 2012.
- [8] M.P.M. Hall, “Effects of the Troposphere on Radio Communication,” *IEEE Electromagnetic Wave Series*, 1979.
- [9] G.A. Hufford, A.G. Longley, W.A. Kissick, “[A Guide to the Use of the ITS Irregular Terrain Model in the Area Prediction Mode](#),” *NTIA Report 82-100*, Apr. 1982.
- [10] W. Feller, *An Introduction to Probability and Its Applications*, Vol. 1, New York, New York: John Wiley & Sons, Inc., 1968, p. 184.
- [11] R. Dalke, “[Statistical Considerations for Noise and Interference Measurements](#),” *NTIA Technical Report TR-09-458*, Nov. 2008.
- [12] H. Cramer, *Mathematical Methods of Statistics*, Princeton, NJ, Princeton University Press, 1946, pp. 507 - 524
- [13] A.D. Spaulding, G.H. Hagn, “[On the Definition and Estimation of Spectrum Occupancy](#),” *IEEE Transactions on Electromagnetic Compatibility*, Vol. EMC-19, No. 3, Aug. 1977.
- [14] J.G. Kemeny, J.L. Snell, *Finite Markov Chains*, D. Van Nostrand Company, Inc., Princeton, 1960.

APPENDIX A: CHANNEL OCCUPANCY IN THE CONTEXT OF RENEWAL THEORY

Following Feller [10], we develop the concept of channel occupancy in the context of renewal theory. We first set up the problem and establish nomenclature. Next, we demonstrate that the quantity of interest satisfies the renewal equation. Finally, we solve the resulting renewal equation in the limit as time goes to infinity. Interested readers are referred to [10] for further explanation and details on the subject. Regarding nomenclature in this appendix: bold fonts denote random variables and processes and unspecified limits on integrals and summations imply limits of 0 to ∞ .

A.1 Setup

As illustrated in Figure A-1, we let $X(t)$ be a binary two-stage renewal process. The defining property of a renewal process is that it starts over independently of the past at each renewal. Two-stage refers to the two events, i.e., $\{X(t) = 1\}$ and $\{X(t) = 0\}$, that must occur in each renewal period. Let V equal the sojourn time for $\{X(t) = 1\}$, and W equal the sojourn time for $\{X(t) = 0\}$. We assume V and W are independent random variables with probability density functions (pdfs) f_V and f_W and cumulative distribution functions (cdfs) F_V and F_W , respectively.

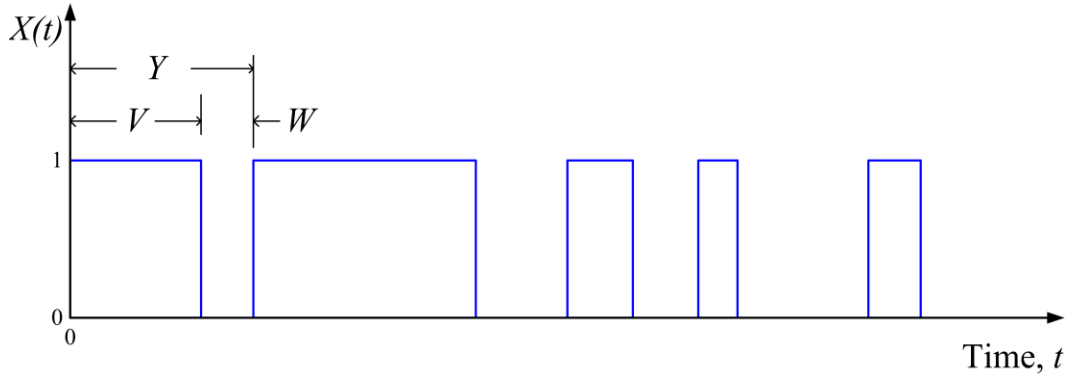


Figure A-1. Renewal process $X(t)$ and associated transmission interval random variables.

Then $Y = V + W$ is the recurrence time with pdf

$$f_Y(y) = [f_V * f_W](y) = \int f_W(y - z)f_V(z)dz, \quad (\text{A-1})$$

and cdf

$$F_Y(y) = [F_V * F_W](y) = \int F_W(y - z)dF_V(z). \quad (\text{A-2})$$

Note that $dF_V(z) = f_V(z)dz$. Also, notice the subtle difference in the convolution operators $*$ versus \star , where (A-2) could be written with $[f_V * F_W](y) = [F_V \star F_W](y)$. Convolutions (in both senses) are associative and linear. In general, the \star convolution between a distribution and continuous function is not commutative, i.e., the order of the terms is important. The \star convolution between distributions, however, is commutative as is the $*$ convolution in general.

To be more explicit with each individual recurrence event as illustrated in Figure A-2, Y_k are independent identically distributed (iid) random variables. The epoch of the m^{th} recurrence is $S_m = Y_1 + Y_2 + \dots + Y_m$ with cdf

$$F_{S_m} = F_Y \star F_Y \star \dots \star F_Y = F_Y^{m\star} , \quad (\text{A-3})$$

where we use $F_Y^{m\star}$ as a shorthand notation for m \star convolutions of F_Y [10].

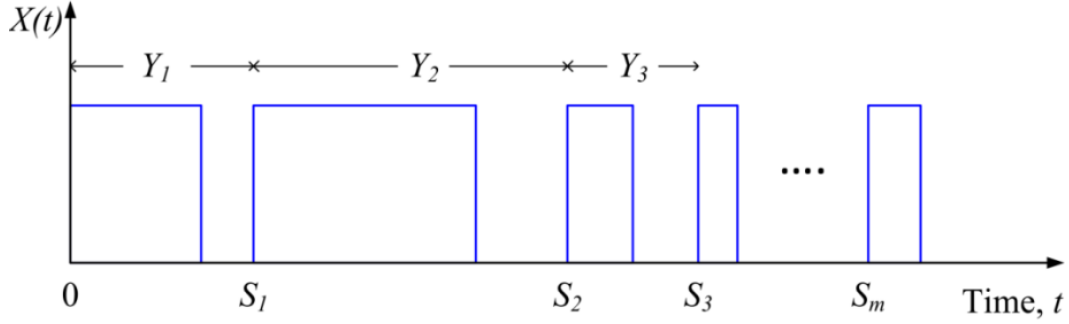


Figure A-2. Sample function of a renewal process.

A fundamental measure in renewal theory is the expected number of renewals, $U(t)$, in the interval $(0, t]$, which we obtain by counting renewal events. More specifically, $N_R(t) = \sum_m \psi_m$ where the random variable $\psi_m = 1$ if and only if $\{S_m \leq t\}$ and equals zero otherwise. Taking the expected value yields

$$\begin{aligned} U(t) &= \mathcal{E}\{N_R(t)\} = \mathcal{E}\left\{\sum_m \psi_m(t)\right\} = \sum_m \mathcal{E}\{\psi_m(t)\} \\ &= \sum_m [1 \cdot \wp\{S_m \leq t\} + 0 \cdot \wp\{S_m > t\}] \\ &= \sum_m F_{S_m}(t) = \sum_m F_Y^{m\star}(t) . \end{aligned} \quad (\text{A-4})$$

A.2 Satisfying the Renewal Equation

In Section 5.1 , we defined channel occupancy as $p(t) = \wp\{\mathbf{X}(t) = 1\}$. We will now show that $p(t)$ satisfies a renewal equation of the form

$$p(t) = a(t) + \int_0^t p(t-y) dF_Y(y) = a(t) + [F_Y \star p](t) , \quad (\text{A-5})$$

where $a(t)$ is a continuous bounded function for $t \geq 0$.

We can write the unconditional probability of the event $\{\mathbf{X}(t) = 1\}$ in terms of the sum over the events $\{\mathbf{Y} = y\}$ (i.e., the first renewal occurs at time y) as follows

$$p(t) = \int \wp\{\mathbf{X}(t) = 1 | \mathbf{Y} = y\} dF_Y(y) . \quad (\text{A-6})$$

Given that the first renewal event occurs at time y , the process starts anew at $t = y$, hence

$$\wp\{\mathbf{X}(t) = 1 | \mathbf{Y} = y\} = \wp\{\mathbf{X}(t - y) = 1\} = p(t - y) \quad \text{for } t \geq y . \quad (\text{A-7})$$

For times $t < y$, the event $\{\mathbf{X}(t) = 1\}$ occurs if and only if t is within the on-time (i.e., $\{\mathbf{V} > t\}$), hence $\wp\{\mathbf{X}(t) = 1 | \mathbf{Y} = y\} = \wp\{\mathbf{V} > t | \mathbf{Y} = y\}$. Substitution into (A-6) gives

$$\begin{aligned} p(t) &= \int_t^\infty \wp\{\mathbf{V} > t | \mathbf{Y} = y\} dF_Y(y) + \int_0^t p(t - y) dF_Y(y) \\ &= \wp\{\mathbf{V} > t | \mathbf{Y} > t\} \wp\{\mathbf{Y} > t\} + \int_0^t p(t - y) dF_Y(y) . \end{aligned} \quad (\text{A-8})$$

The first integral evaluates as shown because if $y > t$ (as dictated by the range of integration), then the integrand is equivalent to $\wp\{\mathbf{V} > t | \mathbf{Y} = y \text{ and } y > t\} = \wp\{\mathbf{V} > t | \mathbf{Y} > t\}$, which can be pulled out of the integral because there is no dependence on y . The remaining integral evaluates to $\int_t^\infty dF_Y(y) = \wp\{\mathbf{Y} > t\}$. Bayes theorem, $\wp\{\mathbf{A} \text{ and } \mathbf{B}\} = \wp\{\mathbf{A} | \mathbf{B}\} \wp\{\mathbf{B}\} = \wp\{\mathbf{B} | \mathbf{A}\} \wp\{\mathbf{A}\}$, allows us to further simplify with

$$\wp\{\mathbf{V} > t | \mathbf{Y} > t\} \wp\{\mathbf{Y} > t\} = \wp\{\mathbf{Y} > t | \mathbf{V} > t\} \wp\{\mathbf{V} > t\} = \wp\{\mathbf{V} > t\} , \quad (\text{A-9})$$

since the event $\{\mathbf{Y} > t\}$ occurs whenever $\{\mathbf{V} > t\}$, i.e., $\wp\{\mathbf{Y} > t | \mathbf{V} > t\} = 1$. This yields

$$p(t) = \wp\{\mathbf{V} > t\} + \int_0^t p(t - y) dF_Y(y) = \wp\{\mathbf{V} > t\} + [F_Y \star p](t) . \quad (\text{A-10})$$

To obtain this last expression with the \star convolution, the limits of integration were replaced by 0 to ∞ because it is understood that $p(t)$ vanishes on the negative half axis, i.e., $p(t - y) = 0$ for $y > t$. Equation (A-10) shows that $p(t)$ satisfies the renewal equation.

To obtain a solution to the renewal equation, we set $G_V(t) = \wp\{\mathbf{V} > t\}$ and convolve (A-10) with $U(t)$, i.e.,

$$U \star p = U \star G_V + U \star F_Y \star p . \quad (\text{A-11})$$

Recalling that $U(t) = F_Y^{0\star} + F_Y^{1\star} + F_Y^{2\star} + \dots$, the last term in equation (A-11) reduces to

$$\begin{aligned} U \star F_Y \star p &= (F_Y^{1\star} + F_Y^{2\star} + \dots) \star p \\ &= (U - F_Y^{0\star}) \star p = (U - \wp\{S_0 \leq t\}) \star p = (U - 1) \star p \end{aligned} \quad (\text{A-12})$$

where $\wp\{S_0 \leq t\} = 1$ because we assume that the first arrival is at $t = 0$. Substitution and solving for $p(t)$ leads to the following solution

$$p(t) = [U \star G_V](t) = \int_0^t G_V(t-y)dU(y). \quad (\text{A-13})$$

A.3 Asymptotic Behavior of the Renewal Process

In the context of channel occupancy, it suffices to understand the behavior of $p(t)$ after the process has been operating for a long time. Hence, in the limit as $t \rightarrow \infty$, we have

$$\lim_{t \rightarrow \infty} p(t) = - \lim_{t \rightarrow \infty} \int_0^t G_V(z)dU(t-z), \quad (\text{A-14})$$

where the integrand and integral limits result from the change of variable $z = t - y$. Recall that $G_V(z) = 1 - F_V(z)$ is a complementary cdf, which is small as z goes to infinity. To evaluate the differential, the renewal theorem states

$$\lim_{t \rightarrow \infty} \frac{\mathcal{E}\{N_R(t)\}}{t} = \frac{1}{\mathcal{E}\{\mathbf{Y}\}}, \quad (\text{A-15})$$

which can be written on the interval $(a, b]$ as $U(t-a) - U(t-b) \rightarrow (b-a)/\mathcal{E}\{\mathbf{Y}\}$ [10]. Hence, the differential in the limit can be interpreted as

$$dU(t-z) \cong U(t-z) - U(t-z-dz) \rightarrow -\frac{dz}{\mathcal{E}\{\mathbf{Y}\}}, \quad (\text{A-16})$$

Substitution into (A-14) and integration by parts, i.e., $\int_a^b uv' dz = uv|_a^b - \int_a^b u'v dz$ with $u = 1 - F_V$ and $v = z$, gives

$$\lim_{t \rightarrow \infty} p(t) = \frac{1}{\mathcal{E}\{\mathbf{Y}\}} \int [1 - F_V(z)] dz = \frac{1}{\mathcal{E}\{\mathbf{Y}\}} \int u dF_V(u) = \frac{\mathcal{E}\{\mathbf{V}\}}{\mathcal{E}\{\mathbf{Y}\}}, \quad (\text{A-17})$$

hence, $p(t)$ tends to a constant, $\mathcal{E}\{\mathbf{V}\}/\mathcal{E}\{\mathbf{Y}\}$, for large t .

APPENDIX B: CONFIDENCE INTERVALS FOR CHANNEL OCCUPANCY ESTIMATES

To estimate channel occupancy, consider the discrete random variable

$$\xi_j = \mathbf{X}(t_j, \omega) = \begin{cases} 1 & \text{with probability } p \\ 0 & \text{with probability } q = 1 - p \end{cases} \quad (\text{B-1})$$

In this expression, random process $\mathbf{X}(t, \omega)$ is a finite function which, for every $t \in \mathfrak{T}$, is a measurable function of $\omega \in \Omega$. Parameter set \mathfrak{T} represents time variation and Ω is the set of possible outcomes of an experiment [11]. Note that random variables and process are identified with bold font.

Probability p is the unknown fixed³ statistic that we aim to estimate via measurement. Toward that end, we make N observations over time interval T and estimate p as the time average

$$\hat{p} = \frac{1}{N} \sum_{j=1}^N \xi_j = \frac{\mathbf{v}}{N}, \quad (\text{B-2})$$

where $\hat{\cdot}$ denotes an estimate. Estimate \hat{p} is a random variable because it is a function on the probability space consisting of events $\omega \in \Omega$. It is properly described by its pdf $g(\hat{p}, p)$, which can be interpreted as a distribution (that integrates to unity) on the vertical at $(p, 0)$ in the $p - \hat{p}$ plane illustrated in Figure B-1 [12].

Suppose there are two functions $\gamma_1(p)$ and $\gamma_2(p)$ such that

$$\wp\{\gamma_1(p) < \hat{p} < \gamma_2(p)\} = \int_{\gamma_1(p)}^{\gamma_2(p)} g(\hat{p}, p) d\hat{p} = 1 - \varepsilon, \quad (\text{B-3})$$

which defines the interval (for fixed p) that contains estimate \hat{p} with probability $1 - \varepsilon$. Domain $D(\varepsilon)$ is the region situated between $\gamma_1(p)$ and $\gamma_2(p)$ that defines this interval for all possible values of p . Equivalently, $D(\varepsilon)$ can be derived from distributions in the horizontal dimension as

$$\wp\{c_1(\hat{p}) < p < c_2(\hat{p})\} = \wp\{\gamma_1(p) < \hat{p} < \gamma_2(p)\} = 1 - \varepsilon, \quad (\text{B-4})$$

which establishes accuracy of estimate \hat{p} with confidence interval (c_1, c_2) with probability $1 - \varepsilon$.

³ Inherent to p being fixed is the assumption that the discrete random process $\mathbf{X}(t_j, \omega)$ is stationary. A stationary random process is invariant under translation in a parameter of interest, e.g., time. We limit our concern here to wide-sense or weakly stationary processes that have constant mean and variance under translation. It is possible to adequately characterize a random process using measurements over time scales during which the process is approximately stationary. In general, however, spectrum usage processes are non-stationary in time due to the human element. Diurnal variations, for example, result from daytime versus nighttime dependencies. There are also weekly variations associated with the typical workweek structure. If it is believed that a statistic changes during the acquisition of data, the data should be separated into subsets and tested for differences, i.e., the statistics are treated as random variables.

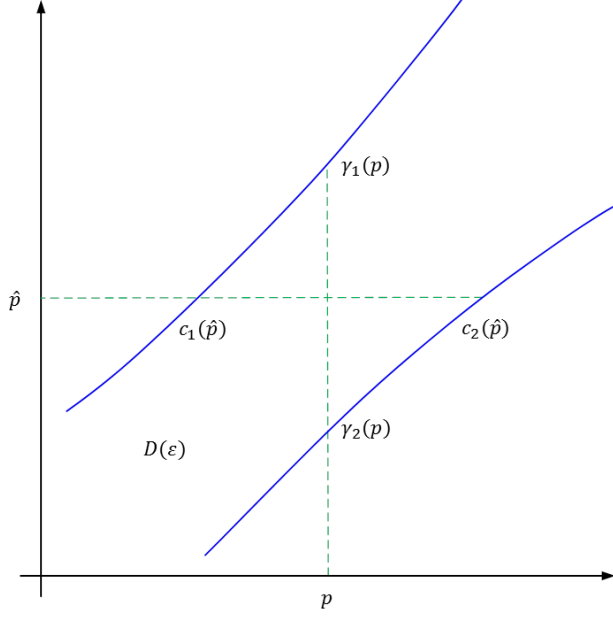


Figure B-1. Illustration of confidence interval (c_1, c_2) for parameter p .

Confidence limits are obtained by taking the inverse of $\gamma_1(p)$ and $\gamma_2(p)$, i.e.,

$$c_1(\hat{p}) = \gamma_2^{-1}(\hat{p}) \quad \text{and} \quad c_2(\hat{p}) = \gamma_1^{-1}(\hat{p}) . \quad (\text{B-5})$$

We need to make some simplifying assumptions about $g(\hat{p}, p)$ in order to obtain expressions for $\gamma_1(p)$ and $\gamma_2(p)$. Recall from (12) that the basis for estimate \hat{p} is counting the number of successes in N Bernoulli trials, i.e., $\mathbf{v} = \xi_1 + \xi_2 + \dots + \xi_N$. In the following subsections, we develop how basic assumptions on independent versus dependent Bernoulli trials can lead to expressions for confidence intervals.

B.1 Assuming Independent Sampling in Time

For a sequence of N independent Bernoulli trials, the number of successes (with probability p) and failures (with probability q) is governed by the binomial distribution, i.e.,

$$\wp\{\mathbf{v} = \ell; N\} = \binom{N}{\ell} p^\ell q^{N-\ell} , \quad (\text{B-6})$$

with $\mathcal{E}\{\mathbf{v}\} = Np$ and $\text{var}\{\mathbf{v}\} = Npq$.

For $Npq \gg 1$ (i.e. large N) and $|\ell - Np|^3 / (Npq)^3 \ll 1$ (i.e., counts reasonably close to the mean) [10], the central limit theorem approximates the pdf of \mathbf{v} as a normal distribution, i.e.,

$$\wp\left\{z_1 < \frac{\mathbf{v} - Np}{\sqrt{Npq}} \leq z_2\right\} \rightarrow \frac{1}{\sqrt{2\pi}} \int_{z_1}^{z_2} e^{-z^2/2} dz = \Phi(z_2) - \Phi(z_1) , \quad (\text{B-7})$$

where $\Phi(\zeta) = \frac{1}{\sqrt{2\pi}} \int_{\zeta}^{\infty} e^{-z^2/2} dz$ is the cdf of the standard normal deviate.

We divide both numerator and denominator of the random variable inside the probability measure by N to provide the normalized distribution of \hat{p} and write the resulting expression in the form of (B-4), i.e.,

$$\wp \left\{ p - z_{\varepsilon} \sqrt{\frac{pq}{N}} < \hat{p} \leq p + z_{\varepsilon} \sqrt{\frac{pq}{N}} \right\} = 1 - \varepsilon \rightarrow 1 - 2\Phi(z_{\varepsilon}) . \quad (\text{B-8})$$

We took the liberty of setting $z_{\varepsilon} = -z_1 = z_2$ (as is customary), which can be calculated for a specified ε via $\varepsilon = 2\Phi(z_{\varepsilon})$. Solutions to this integral equation are accessible via look up table or the complementary error function, i.e., $\Phi(\zeta) = \frac{1}{2} \operatorname{erfc}(\frac{\zeta}{\sqrt{2}})$.

The resulting expressions $\gamma_{2,1}(p) = p \pm z_{\varepsilon} \sqrt{pq/N}$ define $D(\varepsilon)$ as an ellipse in the $\hat{p} - p$ plane. To take the inverse per (B-5), we write the single equivalent expression

$$\hat{p} = p \pm z_{\varepsilon} \sqrt{\frac{pq}{N}} , \quad (\text{B-9})$$

square, and solve the resulting quadratic equation for p . The solution gives the confidence limits for independent sampling, i.e.,

$$c_{2,1}(\hat{p}) = \frac{\hat{p} + \frac{z_{\varepsilon}^2}{2N} \pm z_{\varepsilon} \sqrt{\left(\frac{z_{\varepsilon}}{2N}\right)^2 + \frac{\hat{p}\hat{q}}{N}}}{1 + \frac{z_{\varepsilon}^2}{N}} . \quad (\text{B-10})$$

B.2 Assuming Dependent Sampling in Time

In some cases, when the sample interval is designed to be less than the mean transmission length, the probability of a 1 on the j^{th} trial depends on what happened on the $(j-1)^{\text{th}}$ trial. In this scenario, a more practical simplification is to assume that the measured sequence is reasonably characterized by a first-order Markov chain [13]. The steady-state equations for a first-order Markov chain in matrix form are $[q \ p] = [q \ p] \bar{\Theta}$ (where the overbar denotes a matrix) or written out as

$$\begin{aligned} q &= \wp\{\xi_j = 0\} = q\theta_{00} + p\theta_{10} \\ p &= \wp\{\xi_j = 1\} = q\theta_{01} + p\theta_{11} \end{aligned} , \quad (\text{B-11})$$

where the transition probabilities are defined as

$$\theta_{k\ell} = \wp\{\xi_j = \ell | \xi_{j-1} = k\} \quad (\text{B-12})$$

and $\wp\{\cdot\}$ indicates a conditional probability. For a two-state process, the identity $\theta_{k0} + \theta_{k1} = 1$ applies. Expressions for the transition probabilities are found by solving these four equations and six unknowns in terms of p , q , and θ_{10} , yielding

$$\bar{\Theta} = \begin{bmatrix} \theta_{00} & \theta_{01} \\ \theta_{10} & \theta_{11} \end{bmatrix} = \begin{bmatrix} 1 - p\theta_{10}/q & p\theta_{10}/q \\ \theta_{10} & 1 - \theta_{10} \end{bmatrix}. \quad (\text{B-13})$$

Note that $2q \geq \theta_{10}$, or alternatively $p \leq (1 + \theta_{11})/2$, is a condition for the Markov process to exist. Otherwise, if $\theta_{10} > 2q$, then $\theta_{01} = p\theta_{10}/q > 2p$, which results in a transition probability (either θ_{10} or θ_{01} depending on p) that exceeds unity.

The Central Limit Theorem for Markov Chains [14] states that, for large N , the pdf of \mathbf{v} tends toward a normal distribution with $\mathcal{E}\{\mathbf{v}\} = Np$ and limiting variance

$$\lim_{N \rightarrow \infty} \text{var}(\mathbf{v}) = \alpha N p q, \quad (\text{B-14})$$

where

$$\alpha = \frac{2q}{\theta_{10}} - 1. \quad (\text{B-15})$$

Consequently, the pdf of \mathbf{v} tends toward a normal distribution, i.e.,

$$\wp \left\{ z_1 < \frac{\mathbf{v} - Np}{\sqrt{\alpha N p q}} \leq z_2 \right\} \rightarrow \frac{1}{2\pi} \int_{z_1}^{z_2} e^{-z^2/2} dz. \quad (\text{B-16})$$

As was done in the in the previous subsection for independent samples, this expression can be written in the form of (B-4), i.e.,

$$\wp \left\{ p - z_\varepsilon \sqrt{\frac{\alpha p q}{N}} < \hat{p} \leq p + z_\varepsilon \sqrt{\frac{\alpha p q}{N}} \right\} = 1 - \varepsilon \rightarrow 1 - 2\Phi(z_\varepsilon), \quad (\text{B-17})$$

where $\gamma_{2,1}(p) = p \pm z_\varepsilon \sqrt{\alpha p q / N}$ define $D(\varepsilon)$. To take the inverse, we write the equivalent expression

$$\hat{p} = p \pm z_\varepsilon \sqrt{\frac{\alpha p q}{N}}, \quad (\text{B-18})$$

square, and solve the resulting quadratic equation for p . The solution gives the confidence limits for dependent sampling as

$$c_{2,1}(\hat{p}) = \frac{\hat{p} + \frac{\alpha z_\varepsilon^2}{2N} \pm z_\varepsilon \sqrt{\left(\frac{\alpha z_\varepsilon}{2N}\right)^2 + \frac{\alpha \hat{p} \hat{q}}{N}}}{1 + \frac{\alpha z_\varepsilon^2}{N}}. \quad (\text{B-19})$$

Figure B-2 illustrates $D(\varepsilon)$ for $\varepsilon = 0.1$ and $N = 738$ (corresponding to the number of weekday measurements acquired during the June 2012 San Diego measurement effort presented in the main body of this report). This plot demonstrates the dependence on p and θ_{11} as well as the difference between independent and dependent sampling. Note that the confidence interval increases as θ_{11} increases, which corresponds to an increase in the correlation between samples. Also observe the $p \leq (1 + \theta_{11})/2$ constraint at the right side of the plot.

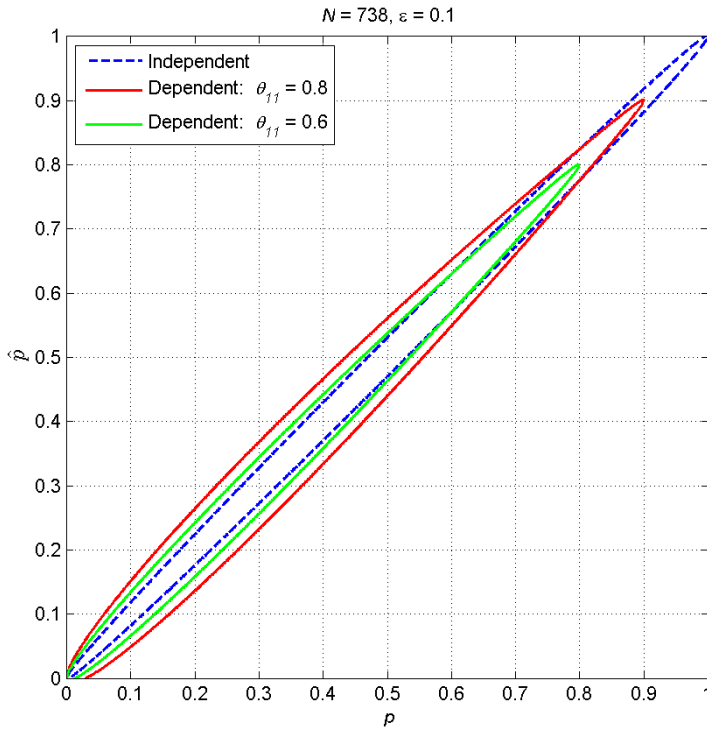


Figure B-2. $D(\varepsilon)$ for $N = 738$ and $\varepsilon = 0.1$ demonstrating the difference between independent and dependent sampling.

APPENDIX C: DAILY SIGNAL-LEVEL AND BAND OCCUPANCY PLOTS

This appendix provides daily signal level and band occupancy statistics calculated for the 3.55–3.65 GHz band measured near San Diego, CA, in June 2012.

Odd numbered plots provide daily maximum, median, minimum, and mean (M4) signal level statistics versus frequency. M4 statistics are calculated using all frequency-swept measurements over a 24 hour period. Means are computed in linear units and converted to dBm. The horizontal grey band is bounded by mean and peak system noise, i.e., P_n and $Q_n(P_n, t_d, B)$, calculated from the last calibration measurement of each day. Note that minimum, median, and mean statistics are missing from the Monday June 11 plots. This is because the system noise level changed in the middle of that day rendering these statistics invalid. The change in system noise was due to a change in the front-end hardware as discussed in Section 4.1.

Even numbered plots provide time versus frequency spectrogram plots and band occupancy versus time plots. For the spectrograms (upper plots), signal levels are mapped to color and plotted versus time and frequency. The lowest value displayed in the spectrogram color bar is the minimum threshold level $L = -83$ dBm. Vertical grey areas denote measurement down times.

Band occupancy (given in the lower plots) is also calculated at this threshold. A channel is considered occupied when the received power is above the threshold. At a particular measurement time, the number of occupied channels, ν , is divided by the total number of channels, $N_c = 100$, to obtain band occupancy. Band occupancy is shown as blue x's in the lower plots. The red curve is an hourly mean and the daily mean is given in the plot title. The number of measurements performed on a given day, N , is also shown in the title.

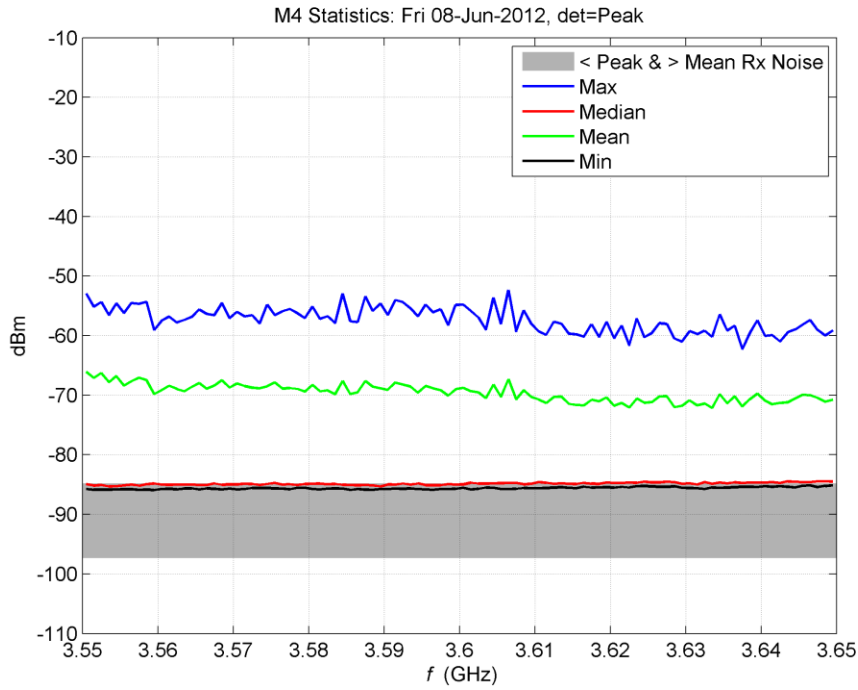


Figure C-1. M4 statistics of 3550–3650 MHz spectrum measured near San Diego on June 8, 2012.

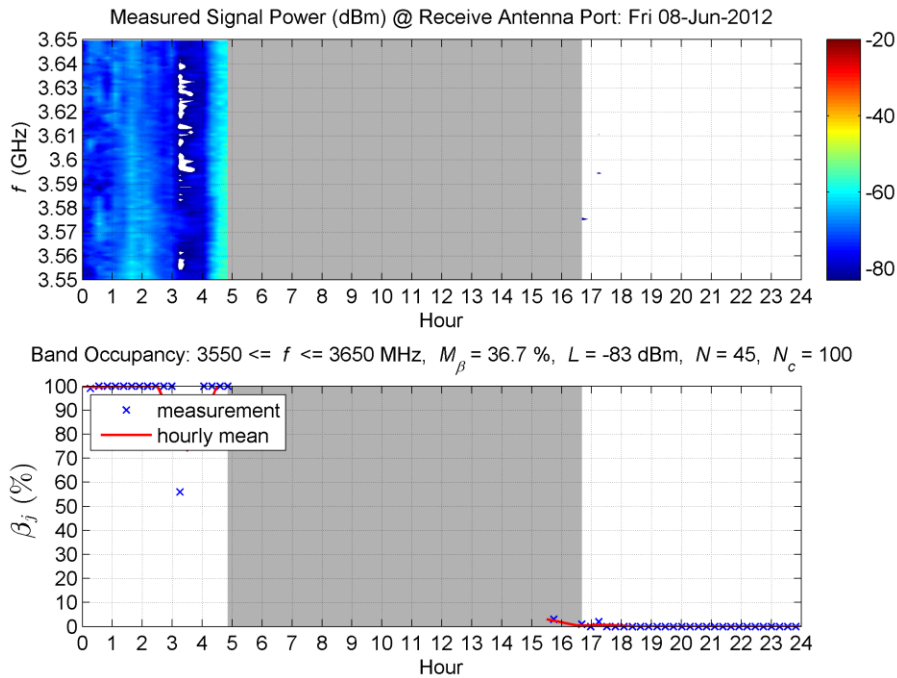


Figure C-2. Spectrogram and band occupancy for 3550–3650 MHz spectrum measured near San Diego on June 8, 2012.

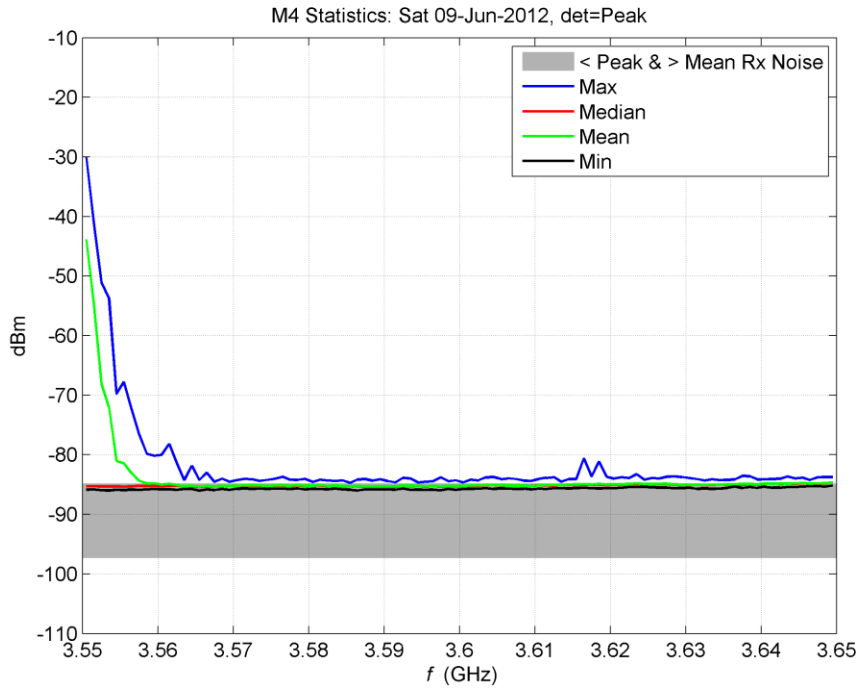


Figure C-3. M4 statistics of 3550–3650 MHz spectrum measured near San Diego on June 9, 2012.

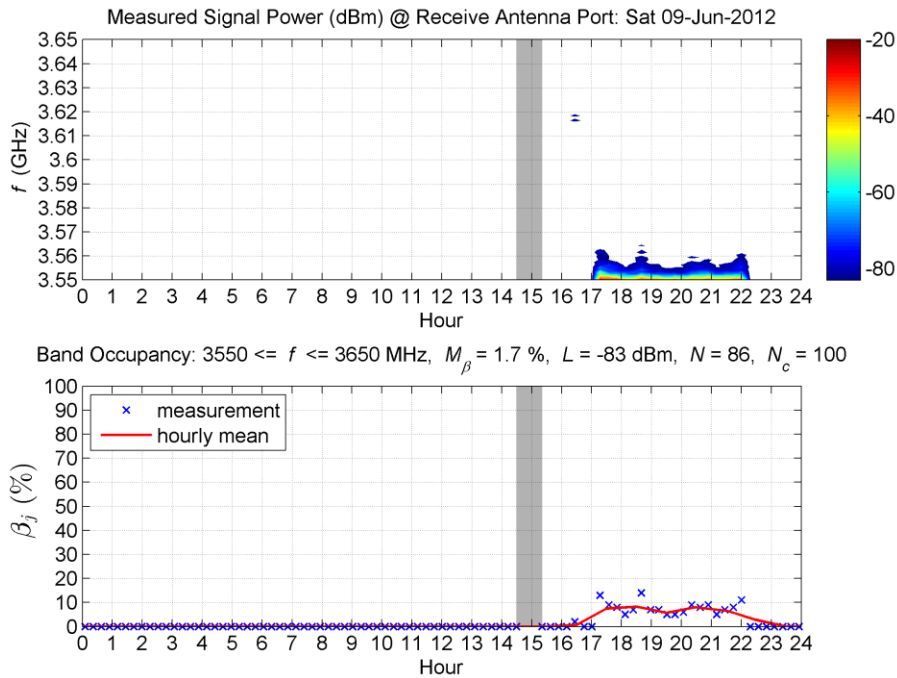


Figure C-4. Spectrogram and band occupancy for 3550–3650 MHz spectrum measured near San Diego on June 9, 2012.

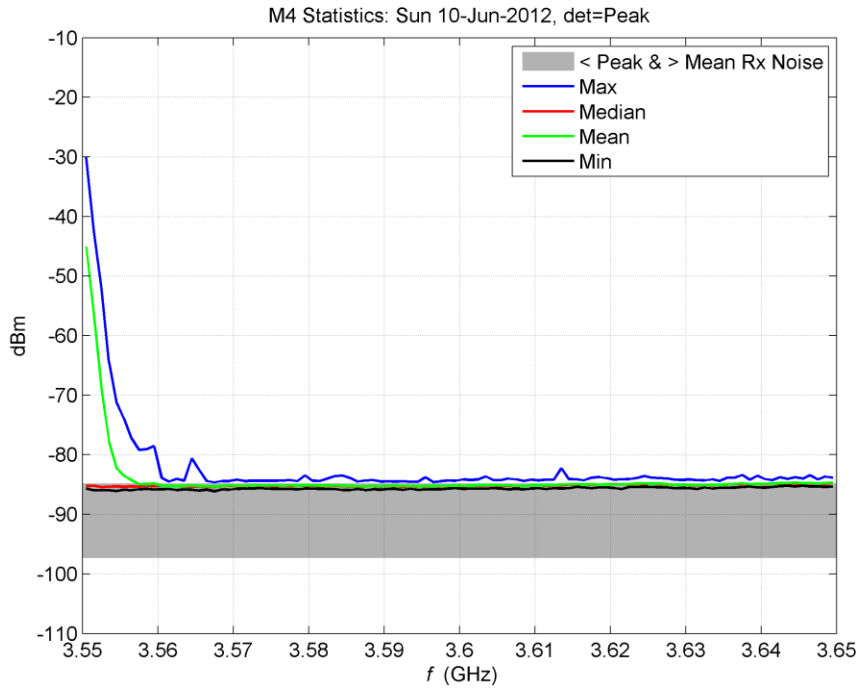


Figure C-5. M4 statistics of 3550–3650 MHz spectrum measured near San Diego on June 10, 2012.

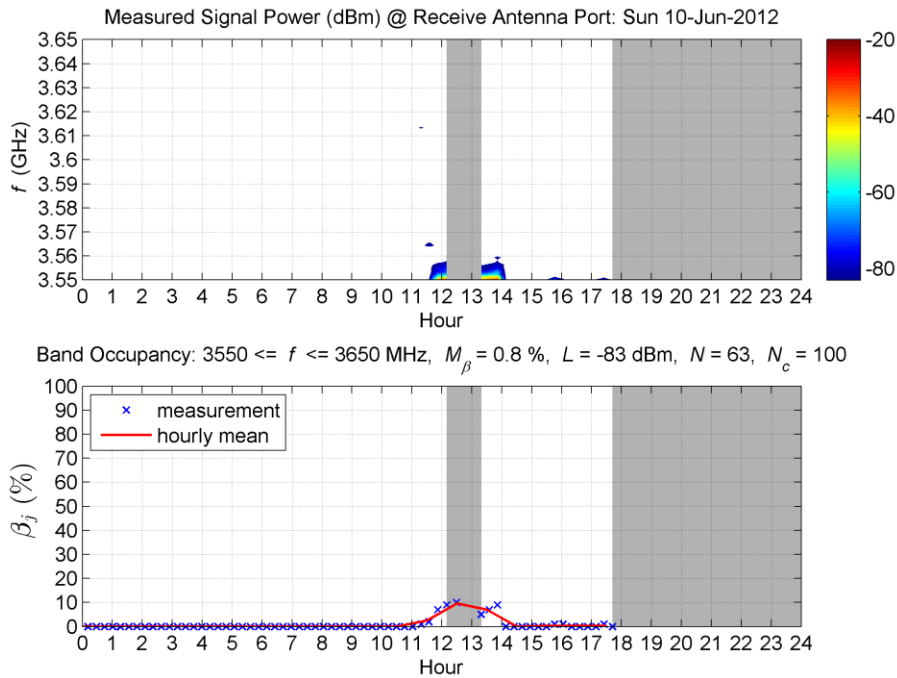


Figure C-6. Spectrogram and band occupancy for 3550–3650 MHz spectrum measured near San Diego on June 10, 2012.

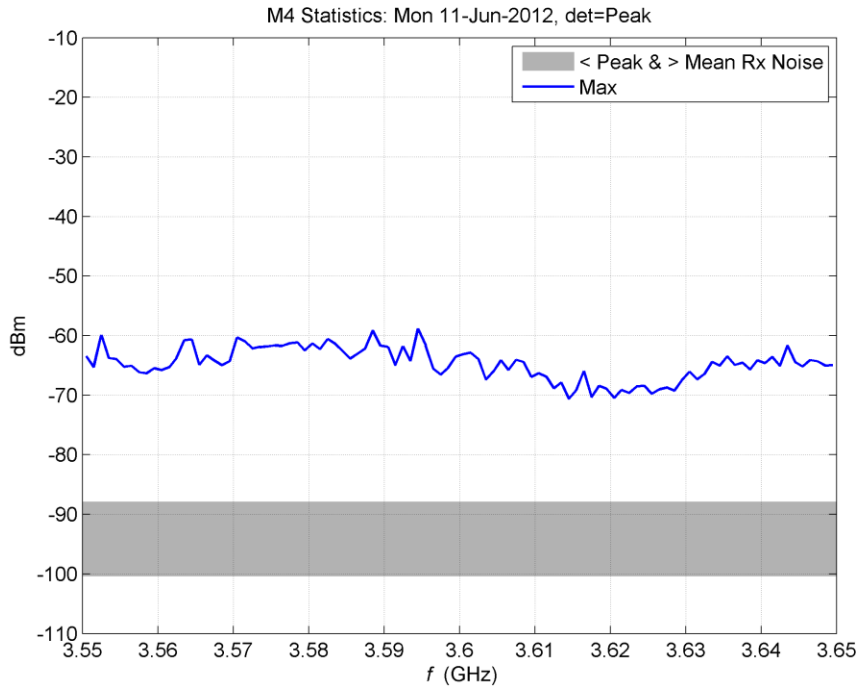


Figure C-7. M4 statistics of 3550–3650 MHz spectrum measured near San Diego on June 11, 2012.

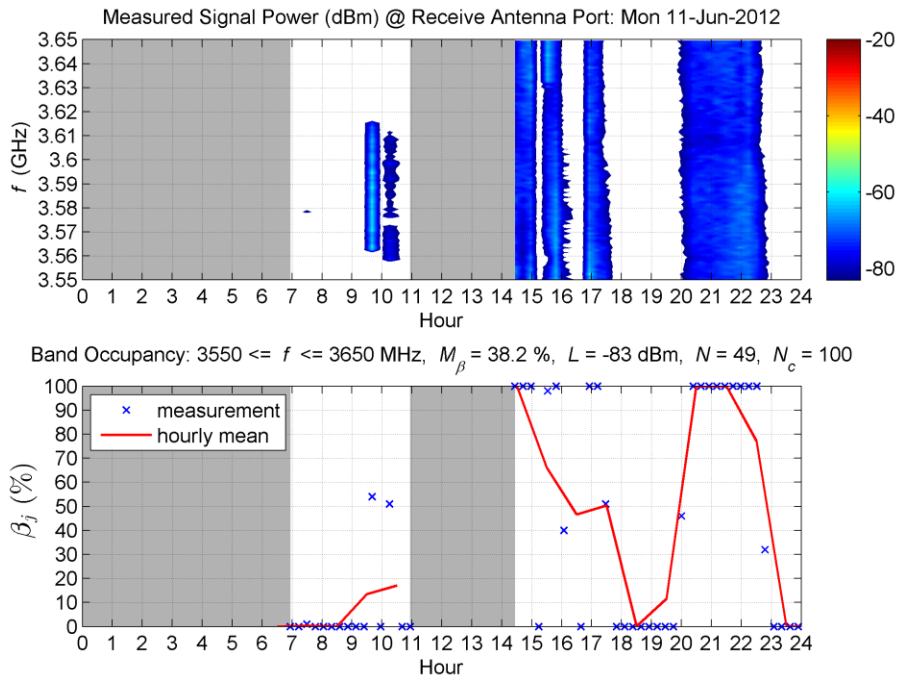


Figure C-8. Spectrogram and band occupancy for 3550–3650 MHz spectrum measured near San Diego on June 11, 2012.

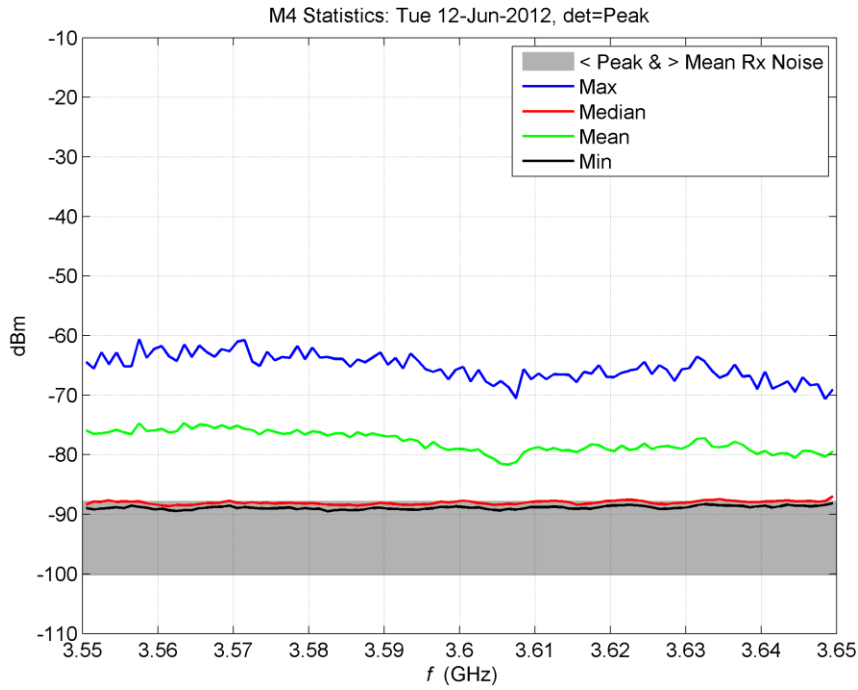


Figure C-9. M4 statistics of 3550–3650 MHz spectrum measured near San Diego on June 12, 2012.

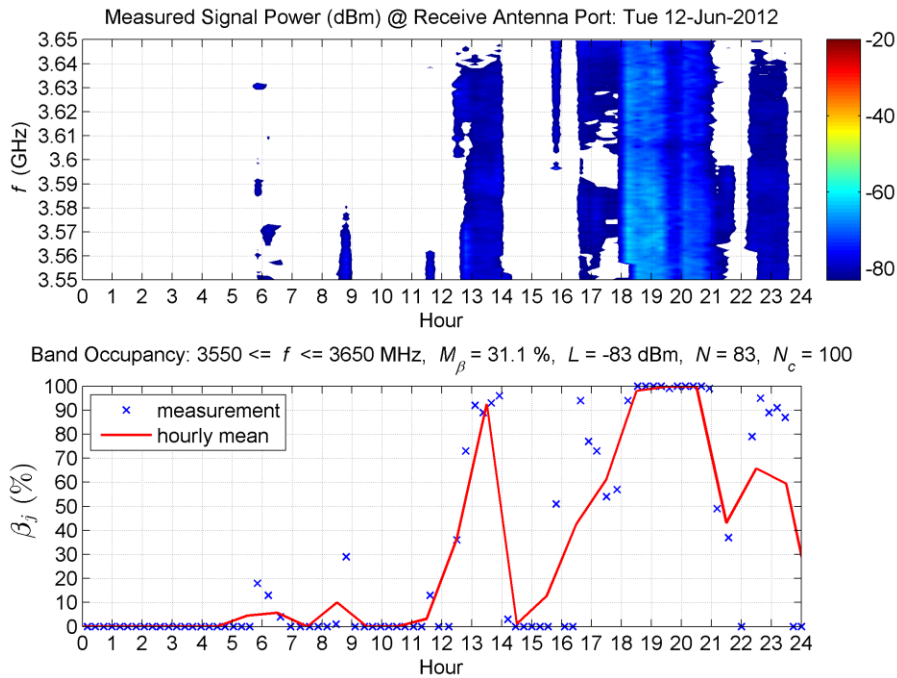


Figure C-10. Spectrogram and band occupancy for 3550–3650 MHz spectrum measured near San Diego on June 12, 2012.

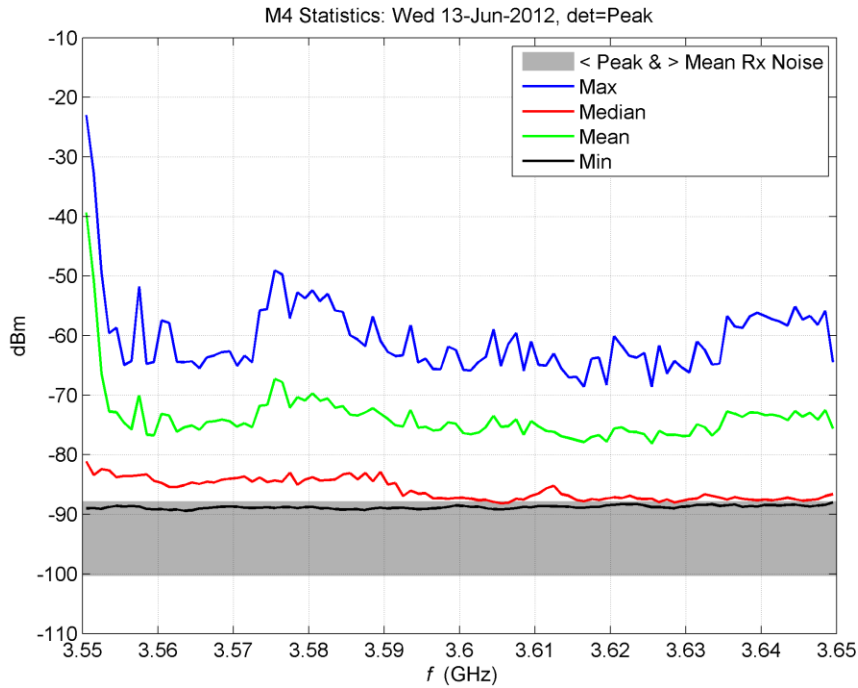


Figure C-11. M4 statistics of 3550–3650 MHz spectrum measured near San Diego on June 13, 2012.

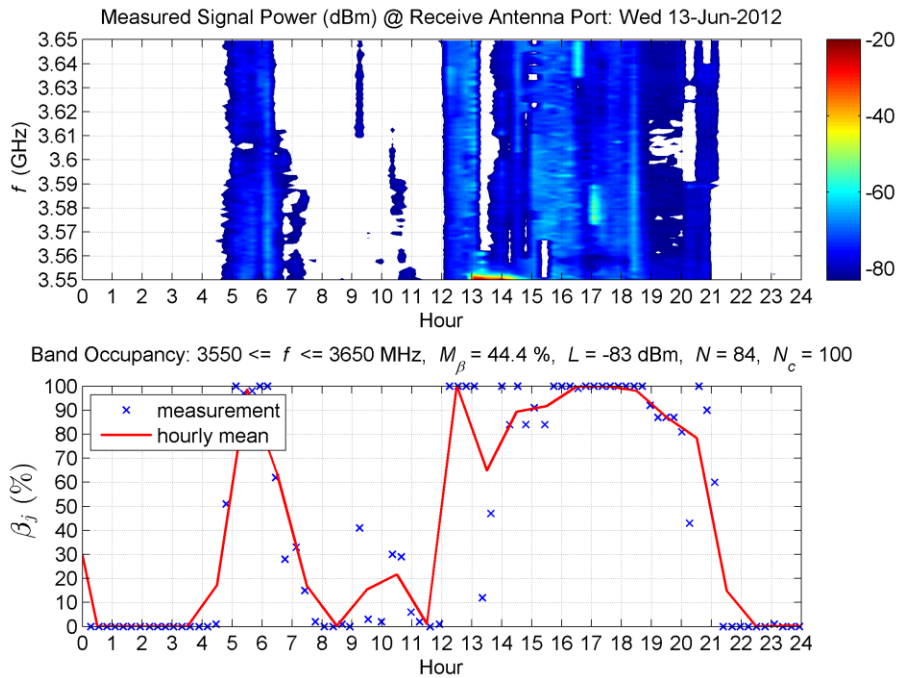


Figure C-12. Spectrogram and band occupancy for 3550–3650 MHz spectrum measured near San Diego on June 13, 2012.

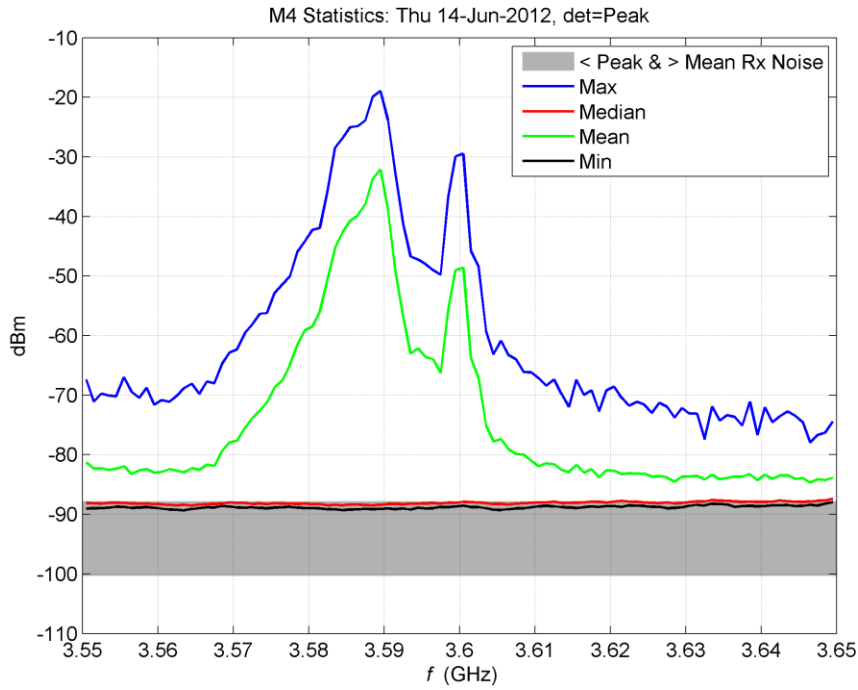


Figure C-13. M4 statistics of 3550–3650 MHz spectrum measured near San Diego on June 14, 2012.

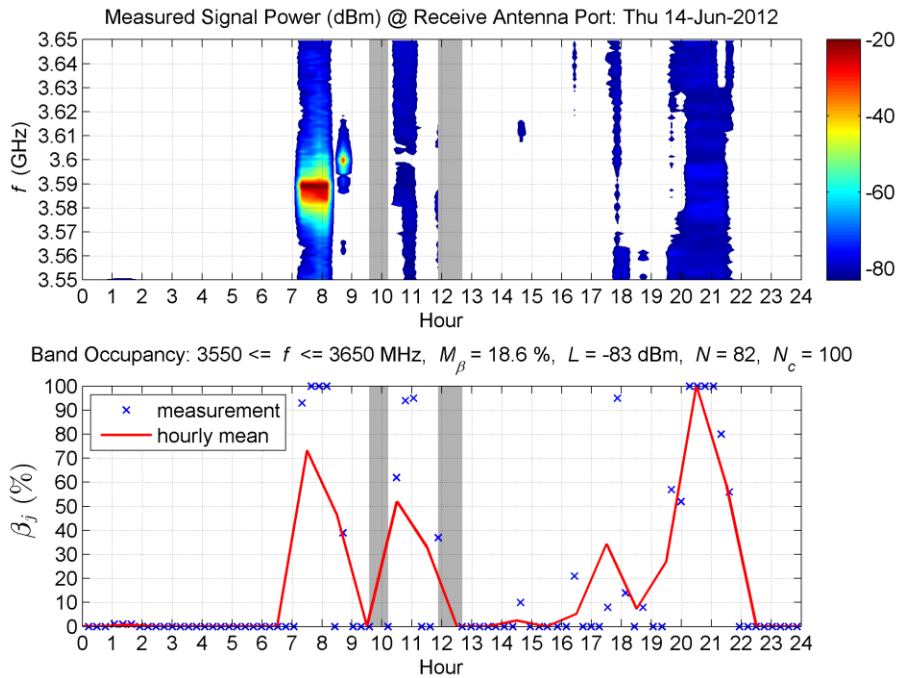


Figure C-14. Spectrogram and band occupancy for 3550–3650 MHz spectrum measured near San Diego on June 14, 2012.

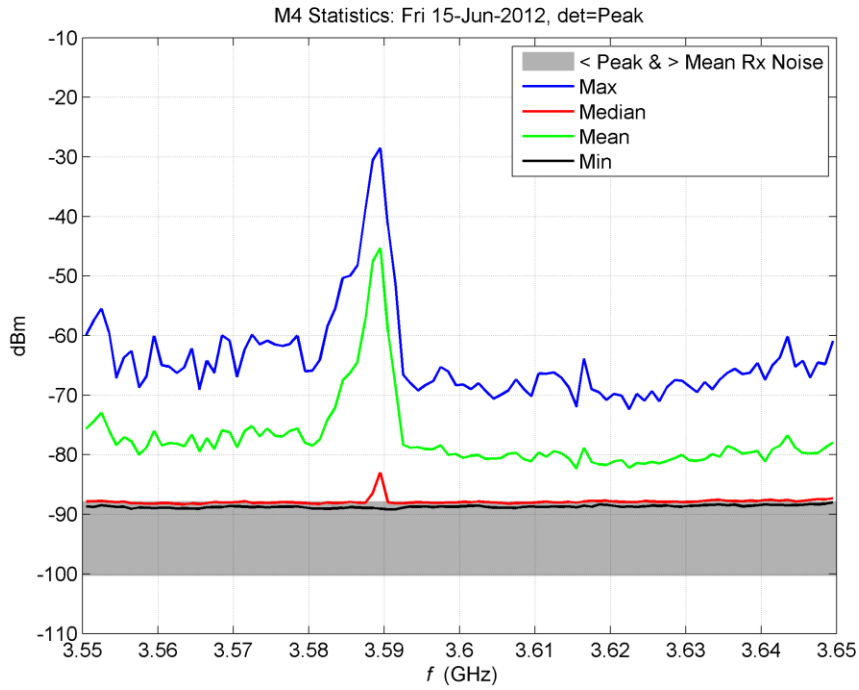


Figure C-15. M4 statistics of 3550–3650 MHz spectrum measured near San Diego on June 15, 2012.

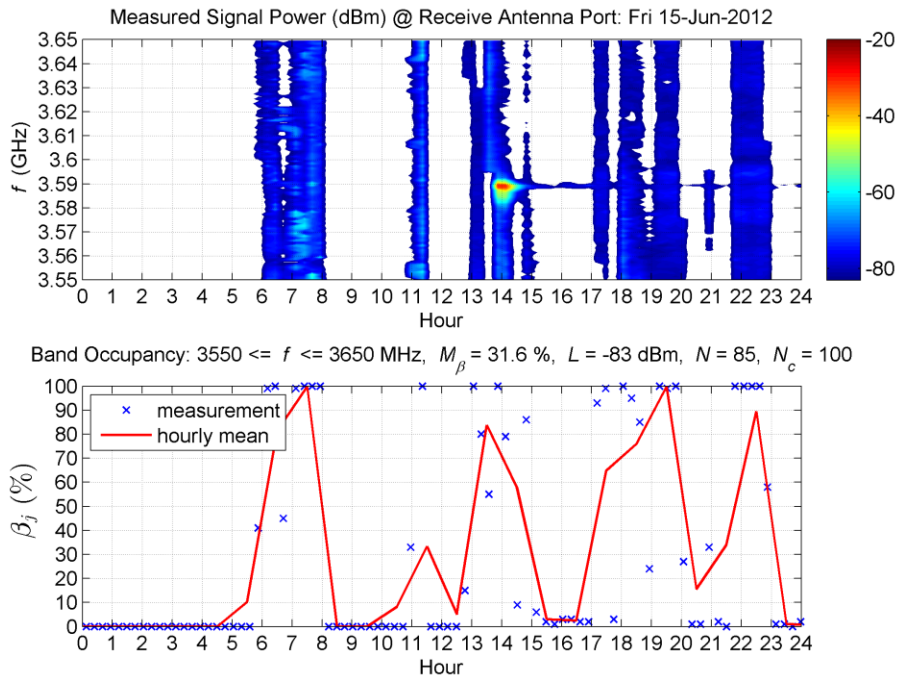


Figure C-16. Spectrogram and band occupancy for 3550–3650 MHz spectrum measured near San Diego on June 15, 2012.

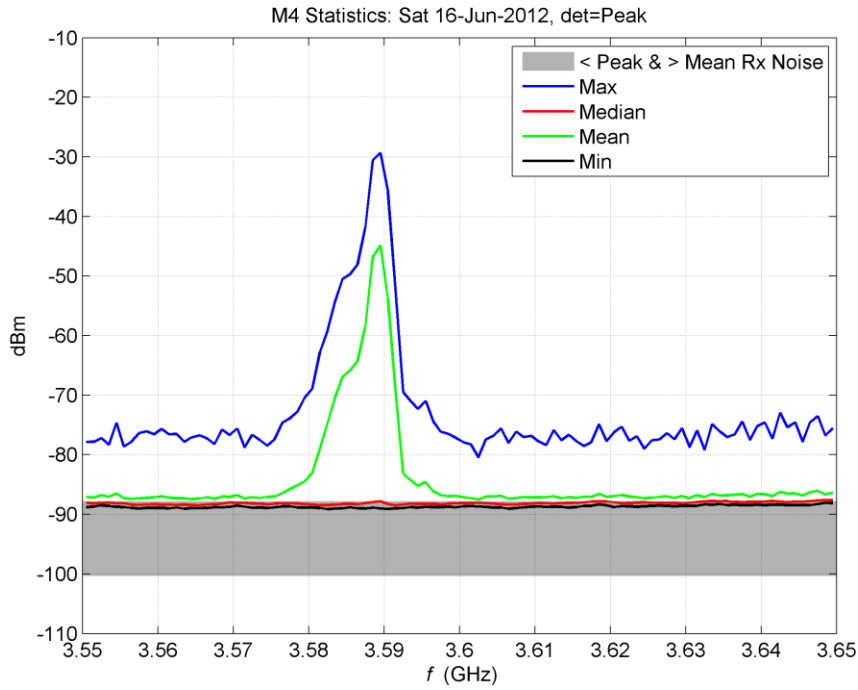


Figure C-17. M4 statistics of 3550–3650 MHz spectrum measured near San Diego on June 16, 2012.

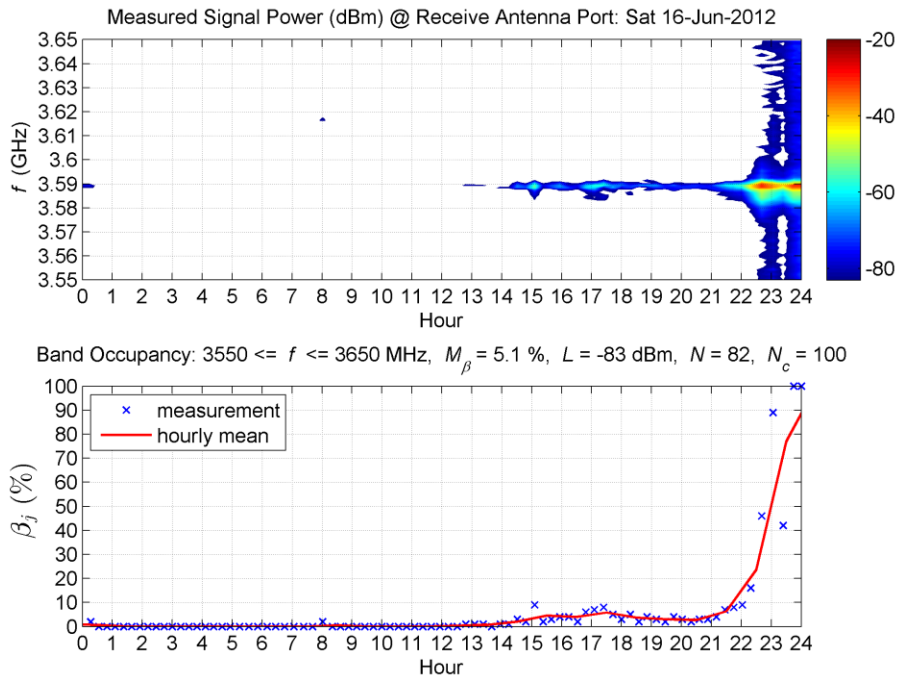


Figure C-18. Spectrogram and band occupancy for 3550–3650 MHz spectrum measured near San Diego on June 16, 2012.

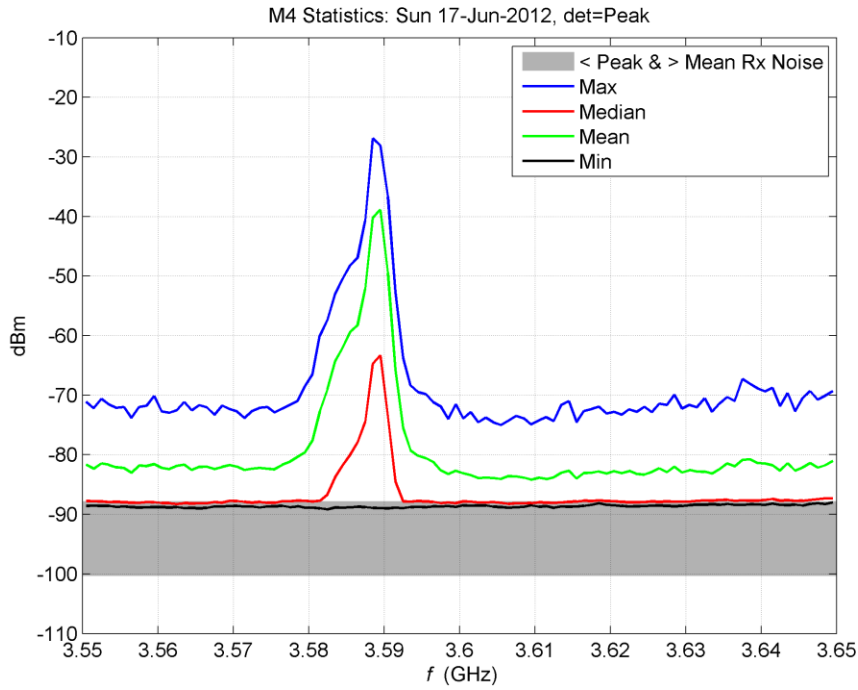


Figure C-19. M4 statistics of 3550–3650 MHz spectrum measured near San Diego on June 17, 2012.

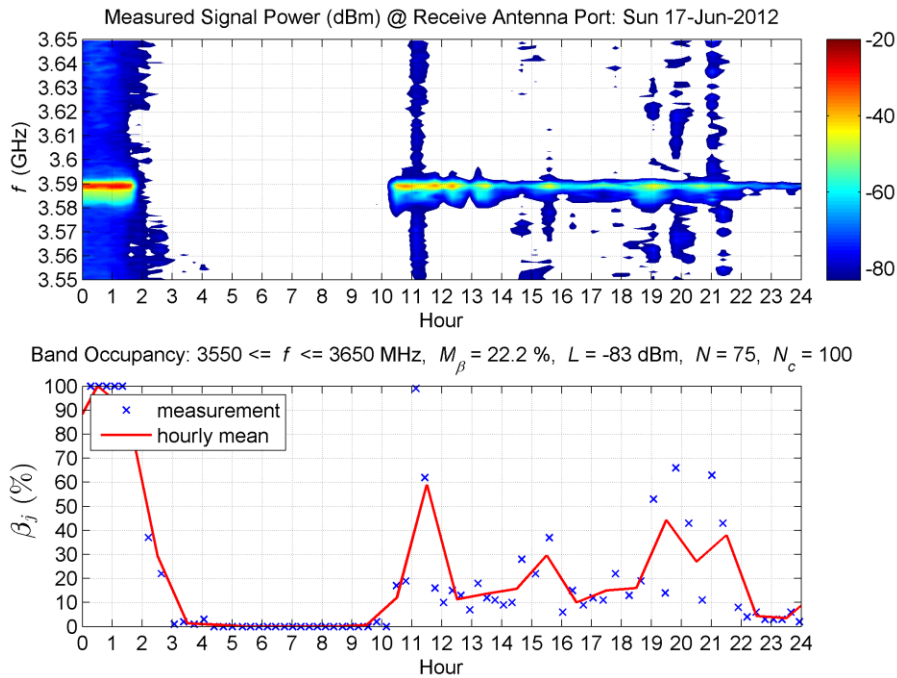


Figure C-20. Spectrogram and band occupancy for 3550–3650 MHz spectrum measured near San Diego on June 17, 2012.

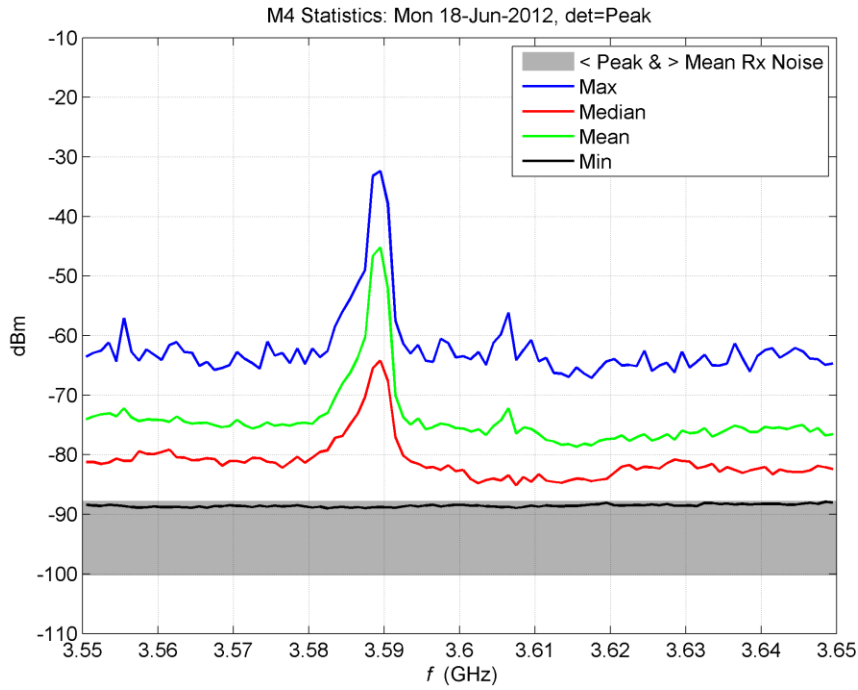


Figure C-21. M4 statistics of 3550–3650 MHz spectrum measured near San Diego on June 18, 2012.

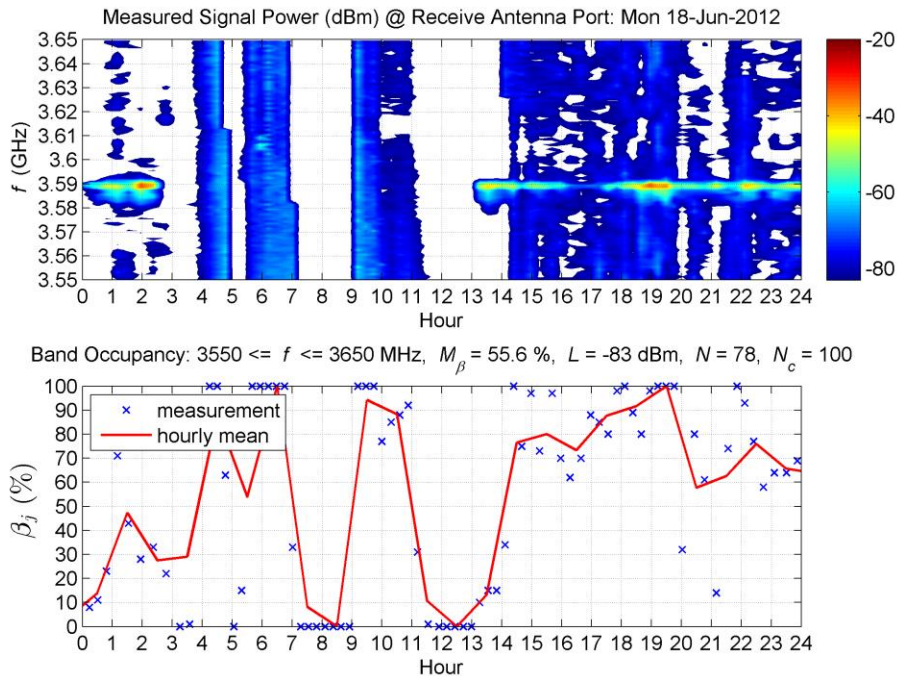


Figure C-22. Spectrogram and band occupancy for 3550–3650 MHz spectrum measured near San Diego on June 18, 2012.

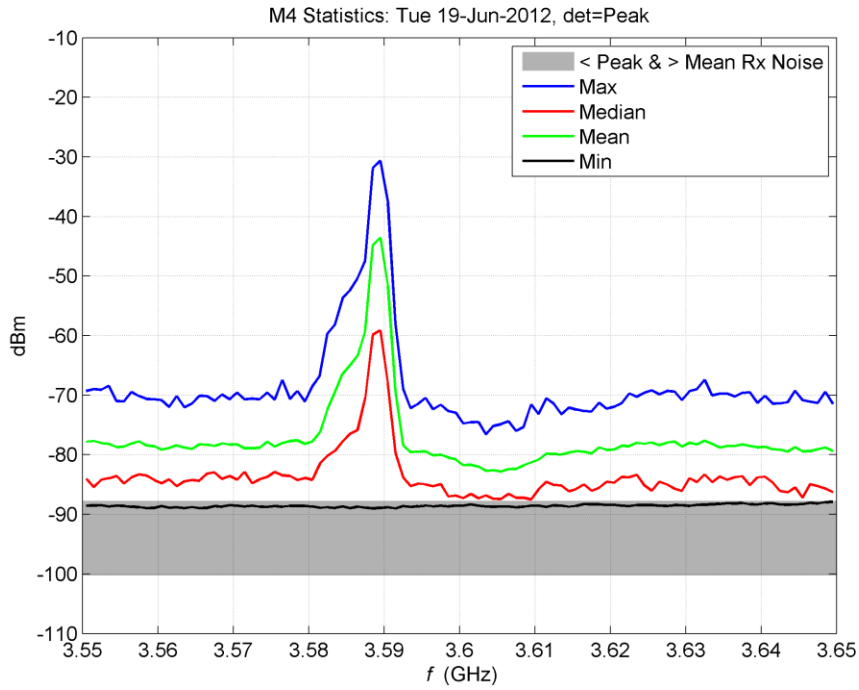


Figure C-23. M4 statistics of 3550–3650 MHz spectrum measured near San Diego on June 19, 2012.

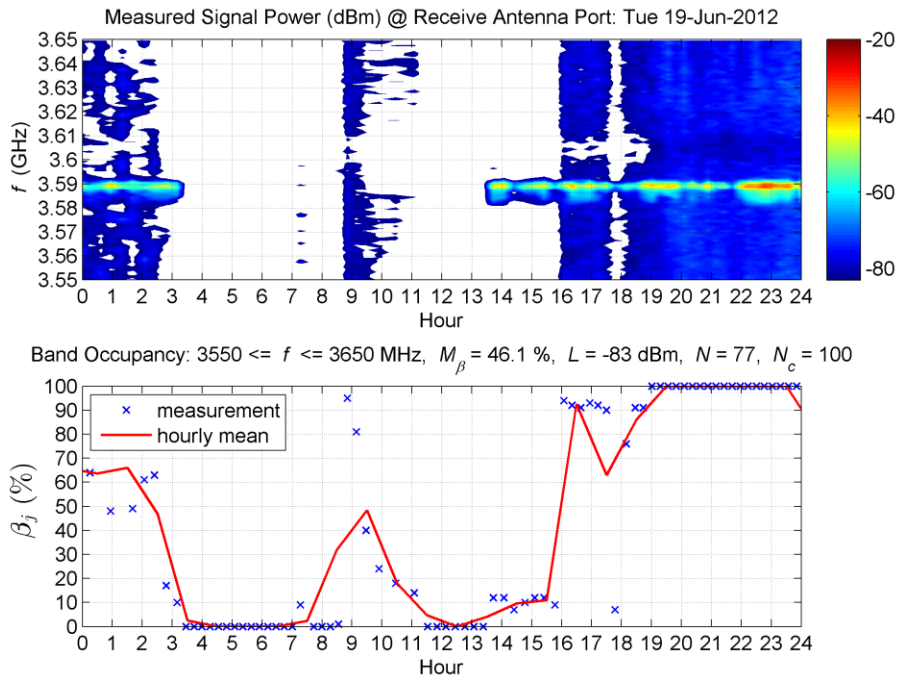


Figure C-24. Spectrogram and band occupancy for 3550–3650 MHz spectrum measured near San Diego on June 19, 2012.

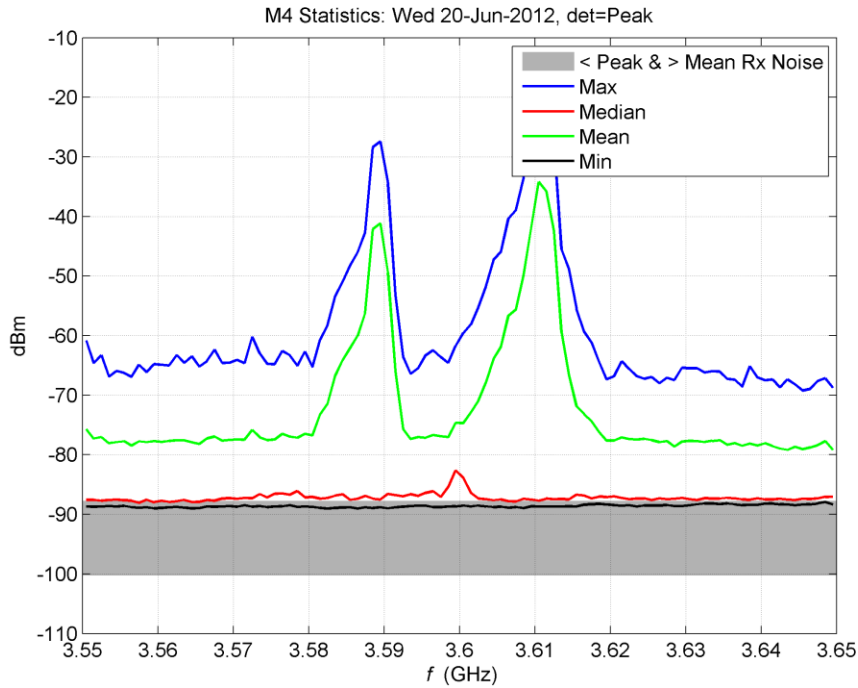


Figure C-25. M4 statistics of 3550–3650 MHz spectrum measured near San Diego on June 20, 2012.

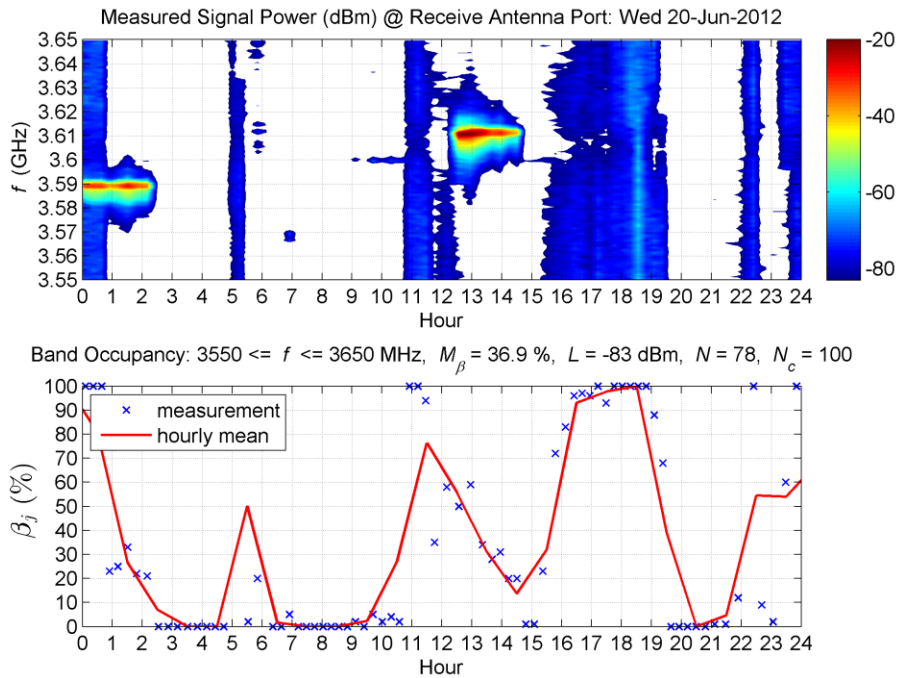


Figure C-26. Spectrogram and band occupancy for 3550–3650 MHz spectrum measured near San Diego on June 20, 2012.

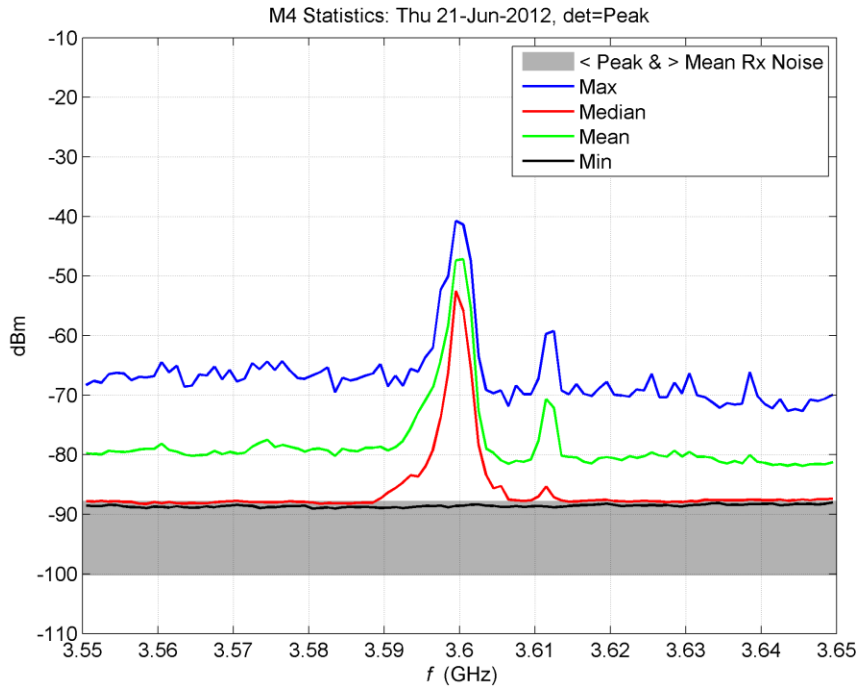


Figure C-27. M4 statistics of 3550–3650 MHz spectrum measured near San Diego on June 21, 2012.

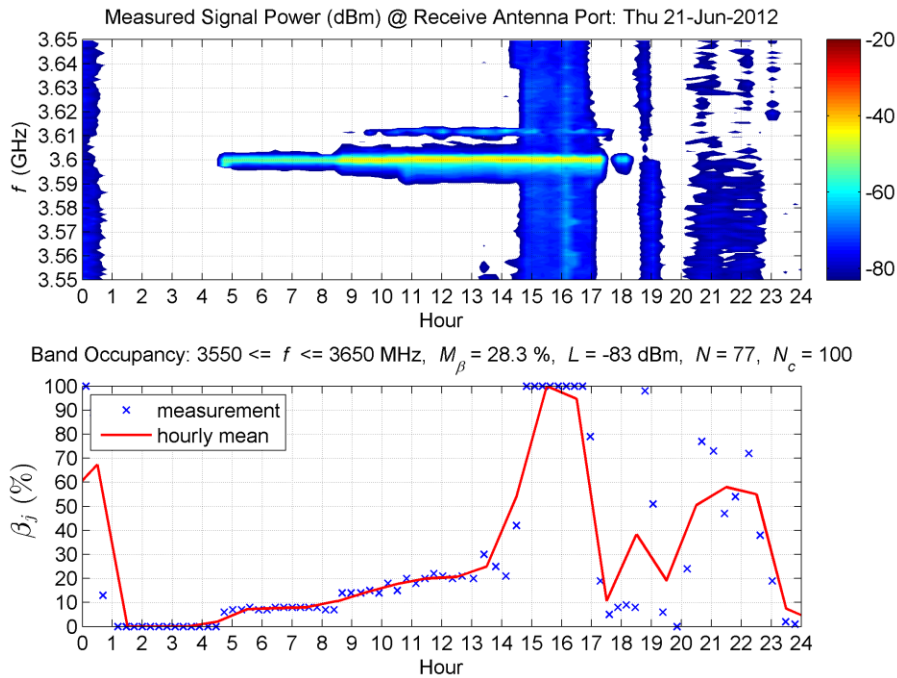


Figure C-28. Spectrogram and band occupancy for 3550–3650 MHz spectrum measured near San Diego on June 21, 2012.

BIBLIOGRAPHIC DATA SHEET

1. PUBLICATION NO. TR-14-500	2. Government Accession No.	3. Recipient's Accession No.
4. TITLE AND SUBTITLE Spectrum Occupancy Measurements of the 3550–3650 Megahertz Maritime Radar Band near San Diego, California		5. Publication Date January 2014
		6. Performing Organization Code ITS.T
7. AUTHOR(S) Michael Cotton and Roger Dalke		9. Project/Task/Work Unit No. 3105012-300
8. PERFORMING ORGANIZATION NAME AND ADDRESS Institute for Telecommunication Sciences National Telecommunications & Information Administration U.S. Department of Commerce 325 Broadway Boulder, CO 80305		10. Contract/Grant No.
		11. Sponsoring Organization Name and Address National Telecommunications & Information Administration Herbert C. Hoover Building 14 th & Constitution Ave., NW Washington, DC 20230
14. SUPPLEMENTARY NOTES		12. Type of Report and Period Covered
15. ABSTRACT (A 200-word or less factual summary of most significant information. If document includes a significant bibliography or literature survey, mention it here.) This report presents spectrum occupancy data of the 3550–3650 megahertz (MHz) maritime radar band measured in June 2012 near San Diego. In this band, the military operates SPN-43 air marshaling radar systems with well-defined signal characteristics. A measurement system and frequency-swept technique were designed specifically to detect SPN-43 emissions. Over the two-week measurement duration in June 2012, we observed multiple systems operating simultaneously in band, spectral spreading of SPN-43 emissions, and out-of-band pulsed emissions that spanned the entire band of interest. In this presumably high-usage mostly military spectrum environment and at a low occupancy threshold (i.e., -83 dBm in a 1 MHz bandwidth at the output of a 2 dBi antenna), mean band occupancy was {36.6, 7.5}% during {weekdays, weekends}. There was a {40.0, 59.8}% chance that the band was empty and a {18.4, 2.3}% chance that the band was full. During weekdays, spectrum usage was dominated by out-of-band pulsed transmissions that spanned the entire band at a relatively low level (approximately 10 dB above the low threshold level). These signals were superimposed on the stronger SPN-43 signals. On average during weekdays, transmissions occurred every four hours with a mean transmission length of approximately 1.5 hours. In contrast, weekend spectrum usage was primarily SPN-43 transmissions at 3.59 GHz arriving every 29 hours (on average) with a mean transmission length of approximately 9 hours. Measured SPN-43 signal amplitudes were at times strong enough to overload the measurement system (exceeding the -83 dBm threshold level by more than 60 dB). Statistical considerations that arise when measured data are used to characterize spectrum occupancy are also discussed in this report. Covered topics include channel occupancy definition, estimation, and uncertainty.		
16. Key Words (Alphabetical order, separated by semicolons) spectrum occupancy, maritime radar, spectrum management		
17. AVAILABILITY STATEMENT <input checked="" type="checkbox"/> UNLIMITED. <input type="checkbox"/> FOR OFFICIAL DISTRIBUTION.	18. Security Class. (This report) Unclassified	20. Number of pages 75
	19. Security Class. (This page) Unclassified	21. Price:

NTIA FORMAL PUBLICATION SERIES

NTIA MONOGRAPH (MG)

A scholarly, professionally oriented publication dealing with state-of-the-art research or an authoritative treatment of a broad area. Expected to have long-lasting value.

NTIA SPECIAL PUBLICATION (SP)

Conference proceedings, bibliographies, selected speeches, course and instructional materials, directories, and major studies mandated by Congress.

NTIA REPORT (TR)

Important contributions to existing knowledge of less breadth than a monograph, such as results of completed projects and major activities. Subsets of this series include:

NTIA RESTRICTED REPORT (RR)

Contributions that are limited in distribution because of national security classification or Departmental constraints.

NTIA CONTRACTOR REPORT (CR)

Information generated under an NTIA contract or grant, written by the contractor, and considered an important contribution to existing knowledge.

JOINT NTIA/OTHER-AGENCY REPORT (JR)

This report receives both local NTIA and other agency review. Both agencies' logos and report series numbering appear on the cover.

NTIA SOFTWARE & DATA PRODUCTS (SD)

Software such as programs, test data, and sound/video files. This series can be used to transfer technology to U.S. industry.

NTIA HANDBOOK (HB)

Information pertaining to technical procedures, reference and data guides, and formal user's manuals that are expected to be pertinent for a long time.

NTIA TECHNICAL MEMORANDUM (TM)

Technical information typically of less breadth than an NTIA Report. The series includes data, preliminary project results, and information for a specific, limited audience.

For information about NTIA publications, contact the NTIA/ITS Technical Publications Office at 325 Broadway, Boulder, CO, 80305 Tel. (303) 497-3572 or e-mail info@its.bldrdoc.gov.